Accepted for publication in the Astronomical Journal
Preprint typeset using LaTeX style emulateapj v. 5/2/11

PHOTOMETRY OF VARIABLE STARS FROM DOME A, ANTARCTICA

Lingzhi Wang[1,2], Lucas M. Macri,[2], Kevin Krisciunas[2], Lifan Wang[2,3], Michael C. B. Ashley[4], Xiangqun Cui[5], Long-Long Feng[3], Xuefei Gong[5], Jon S. Lawrence[4,6], Qiang Liu[7], Daniel Luong-Van[4], Carl R. Pennypacker[8], Zhaohui Shang[9], John W. V. Storey[4], Huigen Yang[10], Ji Yang[3], Xiangyan Yuan[5,11], Donald G. York[12], Xu Zhou[7,11], Zhenxi Zhu[3] & Zonghong Zhu[1]

Accepted for publication in the Astronomical Journal

ABSTRACT

Dome A on the Antarctic plateau is likely one of the best observing sites on Earth thanks to the excellent atmospheric conditions present at the site during the long polar winter night. We present high-cadence time-series aperture photometry of 10,000 stars with $i < 14.5$ mag located in a 23 square-degree region centered on the south celestial pole. The photometry was obtained with one of the CSTAR telescopes during 128 days of the 2008 Antarctic winter.

We used this photometric data set to derive site statistics for Dome A and to search for variable stars. Thanks to the nearly-uninterrupted synoptic coverage, we find 6× as many variables as previous surveys with similar magnitude limits. We detected 157 variable stars, of which 55% are unclassified, 27% are likely binaries and 17% are likely pulsating stars. The latter category includes δ Scuti, γ Doradus and RR Lyrae variables. One variable may be a transiting exoplanet.

Subject headings: astronomical sites: Dome A – photometry: variable stars

1. INTRODUCTION

Long, continuous, unbroken time-series photometry is highly advantageous for a range of astrophysical problems, such as exoplanet searches, studies of periodic variable stars and discoveries of previously-unknown stellar behavior. While these data can be obtained via coordinated observations by a world-wide telescope network, such an approach is fraught with calibration issues, variable weather across the sites, and is highly labor intensive. Ideally, the data would be acquired with a single, fully autonomous robotic telescope. Space is obviously an ideal place to acquire such data due to the high photometric quality and long observing sequences that can be achieved, as demonstrated by the CoRoT (Baglin et al. 2006; Boisnard & Auvergne 2006) and Kepler missions (Benkő et al. 2010; Borucki et al. 2010). Antarctica offers the only location on the surface of the earth where similar observations can be obtained.

The Antarctic plateau offers an unparalleled opportunity to make these types of observations with a single telescope. The combination of high altitude, low temperature, low absolute humidity, low wind and extremely stable atmosphere opens new windows in the infrared and terahertz regions and offers improved conditions at optical and other wavelengths. These advantages offer astronomers gains in sensitivity and measurement precision that can exceed two orders of magnitude over even the best temperate sites (Storey 2005, 2007, 2009; Burton 2010). Additionally, the high duty cycle and long duration of observations from Antarctic sites such as Dome A and Dome C allow for efficient asteroseismic observations. Observations with one site on the Antarctic plateau offers a performance similar to or better than a six-site network at other latitudes (Mosser & Aristidi 2007).

Furthermore, sites on the Antarctic plateau suffer from less high-altitude turbulence than temperate sites and thus enjoy lower scintillation noise leading to superior photometric precision (Kenyon et al. 2006). The elevation of a source observed from Antarctica changes little during the the course of 24 hours, again improving photometric precision and providing the potential for long, continuous time-series observations.

Other advantages include dark skies and lower precipitable water vapor (PWV) which leads to better atmospheric transmission. Some disadvantages that must be considered include aurorae, a reduced amount of the celestial sphere that is available for observations, and prolonged twilight. One site on Antarctica, Dome C, has a similar number of cloud-free astronomically dark time and has lower atmospheric scattering than low-latitude sites, reducing the sky brightness and extinction (Kenyon & Storey 2006).

[1] Department of Astronomy, Beijing Normal University, Beijing, 100875, China
[2] Mitchell Institute for Fundamental Physics & Astronomy, Department of Physics & Astronomy, Texas A&M University, College Station, TX 77843, USA
[3] Purple Mountain Observatory, Chinese Academy of Sciences, Nanjing 210008, China
[4] School of Physics, University of New South Wales, NSW 2052, Australia
[5] Nanjing Institute of Astronomical Optics and Technology, Nanjing 210042, China
[6] Australian Astronomical Observatory, NSW 1710, Australia
[7] National Astronomical Observatory of China, Chinese Academy of Sciences, Beijing 100012, China
[8] Center for Astrophysics, Lawrence Berkeley National Laboratory, Berkeley, CA, USA
[9] Tianjin Normal University, Tianjin 300074, China
[10] Polar Research Institute of China, Pudong, Shanghai 200136, China
[11] Chinese Center for Antarctic Astronomy, Nanjing 210008, China
[12] Department of Astronomy and Astrophysics and Enrico Fermi Institute, University of Chicago, Chicago, IL 60637, USA

A very promising site on the Antarctic plateau is Dome A, at an elevation of 4,093m (840m higher than Dome C), where the Chinese Kunlun station is under construction. Dome A is possibly the best astronomical site on Earth based on data, models, and meteorological parameters such as cloud cover, boundary layer characteristics, aurorae, airglow, free atmosphere, and precipitable water vapor (Saunders et al. 2010, 2009). Swain & Gallée (2006) have modeled the turbulent surface layer across the entire Antarctic ice sheet and found thickness differences from site to site, with one of the thinnest regions being at Dome A. This was confirmed by Snodar measurements in 2009. The median thickness of the boundary layer was 14m (Bonner et al. 2010).

Long-term time-series photometric data has been acquired at the South Pole and at Dome C. The 5-cm South Pole Optical Telescope was used to obtain continuous observations over 78 hours of the Wolf-Rayet star γ^2 Velorum (Taylor 1990). Strassmeier et al. (2008) used the 25-cm sIRAIT telescope to obtain continuous (98% duty cycle over 10 days) photometry of two bright variable stars. The resulting light curves had *rms* scatter of 3 mmag in the V band and 4 mmag in the R band over a period of 2.4hrs, values that are $3-4$ times better than previously obtained with an equivalent telescope in southern Arizona. They attributed the improved photometric precision to the exceptionally low scintillation noise in the Antarctic plateau. The ASTEP project (Crouzet et al. 2010) used a fixed 10 cm refractor to monitor a 15-sq degree field centered on the South Celestial Pole during 4 months of operation (2008 June-September). They found sky conditions suitable for observations were present for $\sim 85\%$ of the time and calculated an observing efficiency for the detection of short-period exoplanets around bright stars that is a factor of $1.5\times$ higher than that of temperate sites.

An observatory that can operate year round without interruptions is required to best capitalize upon the advantages provided by the Antarctic plateau. We have built such an observatory at Dome A, called PLATO (Ashley et al. 2010; Luong-van et al. 2010; Yang et al. 2009; Lawrence et al. 2009; Lawrence et al. 2008; Hengst et al. 2008; Lawrence et al. 2006), and a quad-telescope called CSTAR (the Chinese Small Telescope ARray, Yuan et al. 2008; Zhou et al. 2010b). Based on a large amount of high-quality photometric data obtained during the 2008 Antarctic winter, Zou et al. (2010) undertook a variety of sky brightness, transparency and photometric monitoring observations, while Zhou et al. (2010a) published a catalog of $\sim 10,000$ stars in a field centered on the South Celestial Pole.

This paper presents an independent analysis of the data acquired by CSTAR during the 2008 Antarctic winter season. §2 briefly describes the instrument, observations and data reduction; §3 presents details of the photometric procedure and the astrometric and photometric calibrations; §4 describes the steps followed to obtain high-precision time-series photometry of the brightest 10,000 stars; §5 presents a catalog of variable stars and rough statistics of variable star types; §6 contains our conclusions.

2. OBSERVATIONS AND DATA REDUCTION

2.1. *Observations*

CSTAR (Yuan et al. 2008; Zhou et al. 2010b), a part of the PLATO observatory[13], is the first photometric instrument deployed at Dome A. It was built by astronomers Xu Zhou and Zhenxi Zhu and is composed of four Schmidt-Cassegrain wide field telescopes. Each CSTAR telescope has a field of view 4.5° in diameter with a pupil entrance aperture of 145 mm. Each focal plane contains an ANDOR DV435 $1K \times 1K$ frame-transfer CCD with a pixel size of 13 μm, which translates to a plate scale of $15''/$ pix. Three of the telescopes have g, r, and i filters similar to those used by Sloan Digital Sky Survey (Fukugita et al. 1996). Table 1 of Zhou et al. (2010b) lists the effective wavelength (470nm, 630nm, 780nm) and full width half maximum (140nm, 140nm, 160nm) of the three filters (g, r, i). No filter is used in the fourth telescope. The field of view of the telescopes is very nearly centered on the South Celestial Pole. Since the telescopes are fixed, stars move in circles about the center of the CCD but only traverse a tiny fraction of a pixel during a single exposure. More details on CSTAR can be found in Zhou et al. (2010a,b).

The CSTAR telescopes were installed at Dome A in January 2008. During the following Antarctic winter season, there were technical problems with 3 of the 4 telescopes – those that use the Sloan g, Sloan r, and "open" filters – which prevented them from obtaining any useful data. Fortunately, the fourth telescope (equipped with the Sloan i filter) performed without any significant issues. Observations were conducted from 2008 March 20 through 2008 July 27; during this interval, more than 287,800 frames were acquired with a total integration time of 1,615 hours. The total amount of raw data collected during the observing season was about 350 GB. Table 1 lists the number of images acquired and total exposure time per month, while Table 2 details the different exposure times used during the observing season.

Two groups have carried out independent analyses of the data; one at the National Astronomical Observatories of the Chinese Academy of Sciences Zhou et al. (2010a) and another at Texas A&M University and Beijing Normal University (present work). A comparison of the photometric precision of the two reductions is given in §4.2.

2.2. *Data Reduction*

The preliminary reduction for the raw science images involved bias subtraction, flat fielding, and fringe correction. We used a bias frame obtained during instrument testing in China. We created a sky flat by median combining 160 images with high sky levels ($\geq$ 15,000 ADU) obtained on 2008 March 17.

The bias-subtracted and flat-fielded i-band images contained a residual fringe pattern with peak-to-peak variations of $\sim 1.4\%$ of the sky value. The fringes are due to variations in the thickness of the CCD and strong emission lines in this region of the visible spectrum. An important aspect of these features is that they introduce an additive contribution to the signal and they should be subtracted to perform photometrically consistent measurements.

[13] http://mcba11.phys.unsw.edu.au/∼plato/cstar.html

TABLE 1
Log of observations

Month 2008	# images	Total exp. time (hr)
March	14345	64.4
April	51390	316.4
May	71665	398.1
June	110358	613.1
July	40082	222.7
Total	287840	1614.7

TABLE 2
Exposure times

Start date	End date	Exp. (s)	# images
2008-03-20	2008-03-23	5	7944
2008-03-23	2008-04-11	30	17514
2008-04-11	2008-07-27	20	262382

We created a fringe correction image by carrying out the following two-step process. We selected 3,450 bias-subtracted and flat-fielded images obtained during 2008 March which exhibited a strong fringe pattern. We first masked all saturated pixels (values above 25,000 ADU) and their nearest neighbors. We then carried out PSF photometry using an automated pipeline based on DAOPHOT and ALLSTAR (Stetson 1987). We set the detection threshold to 5σ above sky. We masked the pixels associated with every star detected in each frame, using different radii for different ranges of instrumental magnitude (15 pix for $m < 15$ mag, 10 pix for $15 < m < 17$ mag and 7 pix for $m > 17$ mag). All remaining pixels on the masked images represented contributions from the sky background or stars below our detection threshold (see below). We grouped the images into 23 sets of 150 frames each, placing consecutive images in different sets to minimize the overlap of masked regions. Since the CSTAR telescopes do not track the rotation of the sky, interleaving consecutive images into different sets ensures that the pixels masked due to the presence of stars will fall at different positions on the detector. We normalized every image by its median sky value and median combined each set. We then median combined the 23 intermediate images into an initial fringe correction image.

The initial fringe correction image could be affected by faint stars below the 5σ detection threshold used in the above procedure. In order to remove such objects, we applied a preliminary fringe correction to the input frames and lowered the detection threshold to 2.5σ above sky. We merged the masks obtained in each of the two steps and repeated the combination process described above to obtain a final fringe correction image.

The fringe correction image was subtracted from each science-quality frame in an iterative manner, scaling its amplitude until the residuals in two corner areas of the frame were statistically indistinguishable.

3. PHOTOMETRY

3.1. *Frame selection and photometry*

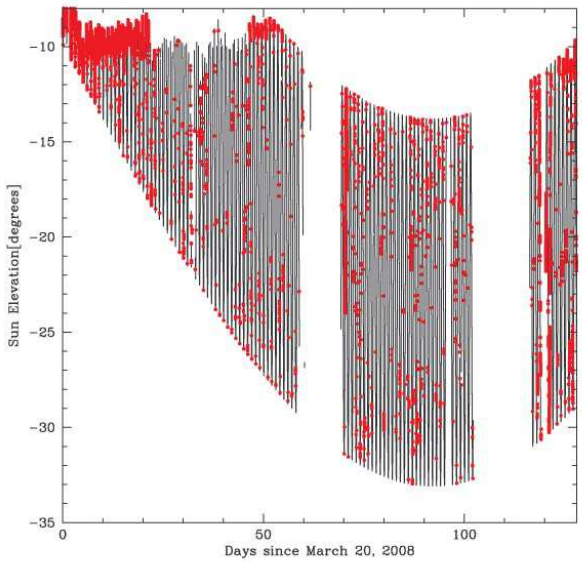

Fig. 1.— Sun elevation angle for each science-quality frame obtained with CSTAR during the Antarctic winter of 2008. Black points indicate frames suitable for analysis, while red points denote frames that failed to meet our selection criteria.

We performed photometry on the debiased, flattened, fringe-corrected images using a pipeline based on DAOPHOT and ALLSTAR. We used the FIND and SKY routines in the IDL version of DAOPHOT to reject images taken under very high sky background or cloudy conditions. We selected frames with a sky level below 6,000 ADU and more than 1,500 stars in the frame; these criteria were met by 93% of the images (about 270,000 frames). Figure 1 shows the distribution of the selected and rejected frames as a function of date and sun elevation angle. 49% of the data obtained in March was rejected due to the high sky background caused by the relatively large sun elevation angle. Only 4%, 5%, 1% and 11% of the data acquired in April, May, June and July, respectively, were rejected. Based on Fig. 1, a suitable initial cut for useful i-band data at Dome A would be a solar elevation angle below $-10°$. 96% of all frames obtained below that value passed our selection criteria.

Frame-by-frame registration was used to combine 3000 of the best images obtained during a 24-hour period of exceptionally good conditions (2008 June 29) to form a master reference image. We selected images with sky values below 500 ADU and with more than 10,000 stars above the detection threshold. We combined the images using MONTAGE (developed by P. Stetson) into a master image that was resampled (via bicubic interpolation) at $4\times$ the initial pixel scale. We restricted the master frame to a circular field of view that was observed continuously, spanning $-90° < \delta < -87°17'$. We masked saturated stars and their surroundings using a circular mask of varying radius. We identified all stars in the masked master image using DAOFIND and a detection threshold of 5σ. The master image is shown in Fig. 2.

Next, we carried out aperture and point-spread function (PSF) photometry using the stand-alone versions of DAOPHOT and ALLSTAR. The aperture photometry radius was set to 2.5 pixels, with the sky annulus ex-

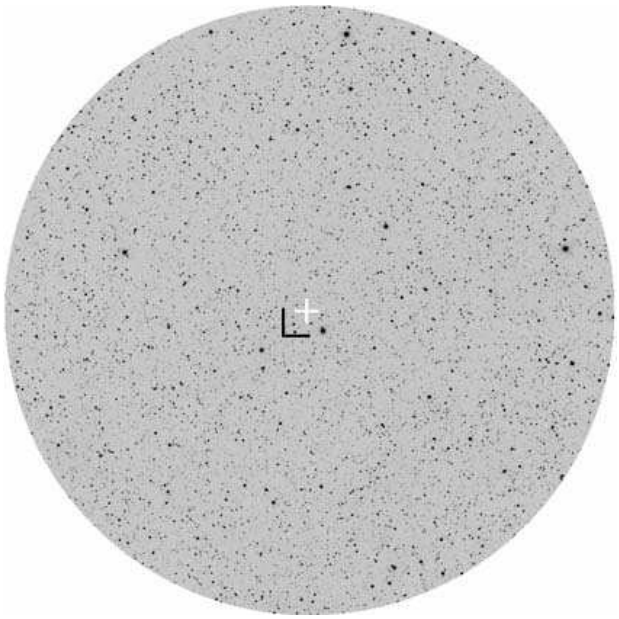

FIG. 2.— Master frame of the CSTAR field of view. The white cross denotes the position of the South Celestial Pole. The edge of the field corresponds to $\delta = -87°17'$. The black lines indicate the bottom-left corner of the inset image shown in Fig. 3.

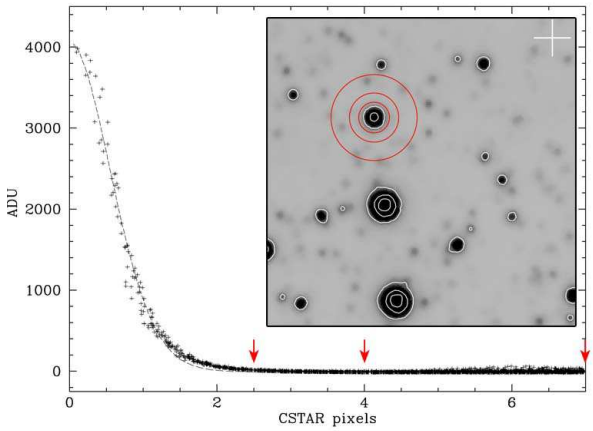

FIG. 3.— Inset: Zoom into a small region of the master image of the CSTAR field (12′ on a side) near the South Celestial Pole (indicated by the white cross as in Fig. 2). The white contours indicate intensity levels logarithmically spaced between 20 and 10^4 ADU. The red circles indicate the extent of the aperture radius and the sky annulus, centered on a random star. Outer plot: radial profile for the same star, indicating the location of the aperture radius and sky annulus.

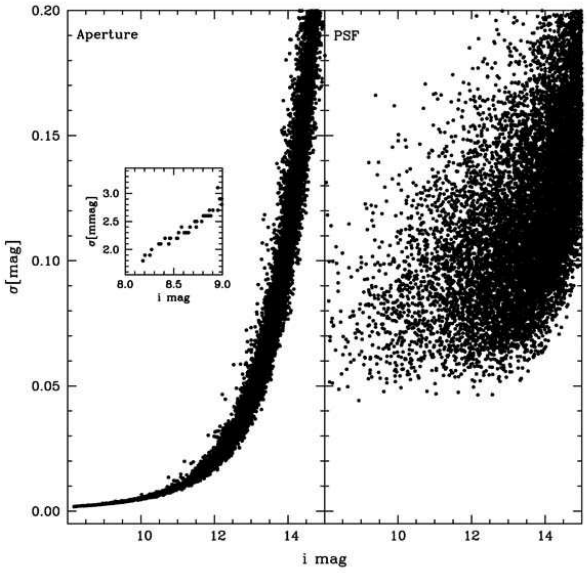

FIG. 4.— Comparison of DAOPHOT/ALLSTAR uncertainties for aperture (left) and PSF (right) magnitudes for a typical frame. The inset zooms in the aperture photometry for $8 < m < 9$.

tending from 4 to 7 pixels. Fig. 3 shows the radial profile and the location of these radii for a random star.

The smallest uncertainties reported by DAOPHOT for aperture photometry were of the order of 2 mmag. We modeled the PSF using a Moffat function with $\beta = 1.5$, which gave the smallest residuals. Due to the severe undersampling of the camera (15″/pix), the smallest uncertainties reported by ALLSTAR for PSF photometry were significantly larger (~ 0.05 mag) than those reported for aperture photometry. Fig. 4 shows a comparison between the reported DAOPHOT aperture and PSF photometric uncertainties. We conclude that PSF photometry is not suitable for the analysis of CSTAR data, and we only use aperture photometry for the remainder of this paper.

We carried out aperture photometry on selected scientific images to determine for each one the number of stars, the sky level, and the photometric zeropoint (proxy for extinction due to clouds) relative to the master frame. The latter was calculated from the magnitude offset of the brightest 1,000 stars in each image across the whole field of view with respect to the corresponding magnitudes in an individual image chosen as our internal photometric reference. Outlier rejections of 3σ were applied iteratively to guarantee the zeropoints were based on non-variable stars. Fig. 5 shows the time series of number of stars, sky level and photometric zeropoint (proxy for differential extinction due to clouds), while Fig. 6 shows the frequencies of occurrence and cumulative density distributions of the same quantities.

There is a small zeropoint offset of ~ 0.03 mag between our reference image and the one used by Zou et al. (2010). Hence, the peak value of the distribution in the top right panel in Fig. 6 is shifted to the left by that amount relative to Fig. 5 of Zou et al. (2010). Based on these values, we can conclude that extinction due to clouds in the i band at Dome A is less than 0.4 mag during 80% of the time and less than 0.1 mag for 50% of the time. Our results are consistent with those presented in Table 1 of Zou et al. (2010).

50% of the science-quality images have at least 7,500 stars above the detection threshold and a sky level below 36 ADU/s. The latter is equivalent to a median sky background of 19.6 mag/□″, consistent with the value of 19.8 mag/□″ derived by Zou et al. (2010). That paper also compared the median sky background from La Palma, Paranal, Cerro Tololo, and Calar Alto and concluded that under moonless clear conditions Dome A has darker sky backgrounds than the above astronomical sites.

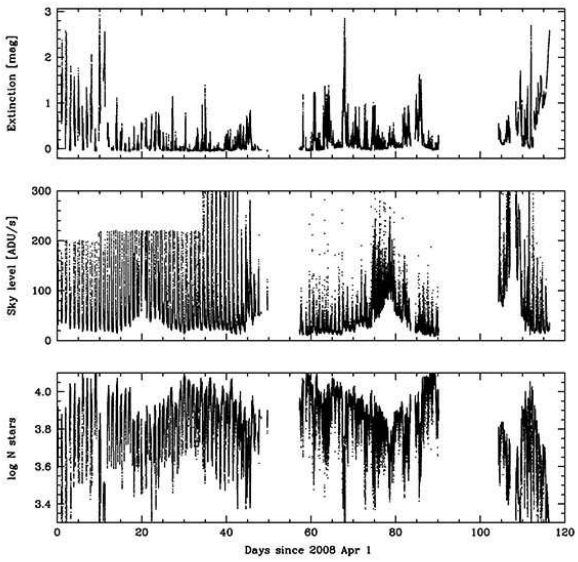

FIG. 5.— Time series plots of differential extinction (top panel), sky brightness level (middle panel), and number of stars on a single image (bottom panel).

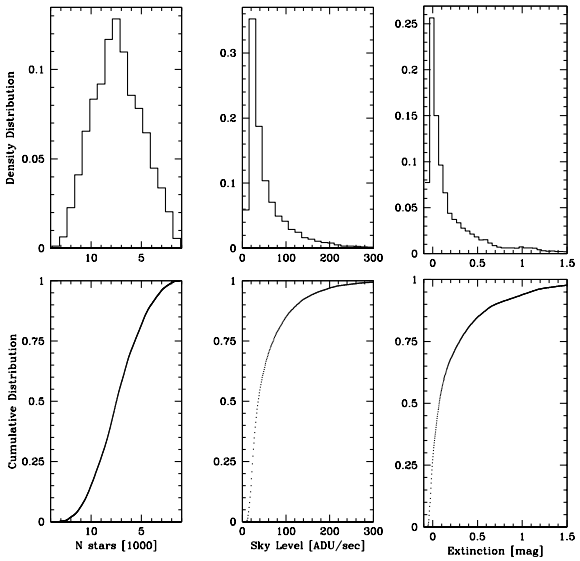

FIG. 6.— Frequency of occurrence and cumulative fraction of the number of stars per image (left column), sky brightness level (middle column), and differential extinction (right column).

3.2. *Astrometric and Photometric calibration*

We determined the astrometric solution of our master reference image based on an independent astrometric calibration of a single frame (15CC0007) obtained during the same observing season by M. Ashley (priv. comm.). We found 5,300 stars in common between this frame and our master reference image using DAOMATCH and DAOMASTER (developed by P. Stetson). We extracted the celestial coordinates of these stars from the calibrated frame using the "xy2sky" routine in WCSTools[14] and determined the astrometric solution of our master reference image using the routines "ccmap" and "ccsetwcs" in IRAF[15]. ccmap was used to compute plate solutions using matched pixel and celestial coordinate lists and ccsetwcs was used to create an image world coordinate system from a plate solution. We used the TNX projection for the WCS of our master reference image.

We determined a mean astrometry uncertainty of $\sim 5''$ ($\sim$ 1/3 pix) by comparing the coordinates we derived and those tabulated in the Guide Star Catalog (version 2.3, Lasker et al. 2008) for selected stars across the entire field of view of our master frame. Fig. 7 shows the distribution of positional differences for these stars.

We determined the photometric calibration of our master reference image using the catalog of calibrated *griz* magnitudes of Tycho stars (Ofek 2008). We used Vizier[16] to select stars with $9 < i < 11.5$ mag and $\delta < -87^\circ$ and matched them to objects in our master image using a positional tolerance of 2.5 pixels ($= 37.5''$). We applied an iterative outlier rejection and determined a photometric zeropoint of 7.46 ± 0.08 mag based on $N = 119$ stars, shown in the bottom panel of Fig. 8.

We checked the above calibration by matching stars in our master frame with bright unblended stars in the catalog of Zhou et al. (2010a), who computed aperture photometry using a 3-pixel radius. Those authors adopted a photometric calibration based on 48 stars in common with the USNO-B catalog, whose i-band magnitudes were determined by Monet et al. (2003). We determined a photometric zeropoint of 7.45 ± 0.04 mag (see top panel of Fig. 8), which is statistically identical to the value determined above.We adopt the calibration based on the Tycho Catalog, as it is based on a larger number of stars.

4. TIME-SERIES PHOTOMETRY

There are approximately 100,000 stars detected in our master reference image, reaching a depth of $i = 20.4$ mag. The brightest 10,000 of these are detected in most individual frames and correspond to the depth of a previous study of this area of the sky by the ASAS project ($V \sim 14.5$ mag Pojmanski 2005). Hence, we selected these objects for time-series photometry with the aim of detecting variable stars and determining the most significant frequencies in their power spectra. Hereafter, we will refer to this subset as the "bright-star sample". We restricted our analysis to the images obtained under the best conditions, defined as a sky background below 50 ADU/s and extinction ≤ 0.5 mag. These conditions were met by 141,700 frames or about 53% of all the science-quality data.

4.1. *Photometric corrections*

We performed a series of corrections to the aperture photometry reported by DAOPHOT, which included: exposure time normalization, zeropoint correction, sigma rescaling, residual flat fielding, time calibration, masking of satellite trails and saturated regions, spike filtering, and magnitude calibration. In greater detail, these corrections entailed the following steps:

[14] http://tdc-www.harvard.edu/wcstools

[15] IRAF is distributed by the National Optical Astronomy Observatory, which is operated by the Association of Universities for Research in Astronomy, Inc., under cooperative agreement with the National Science Foundation (NSF).

[16] http://vizier.u-strasbg.fr

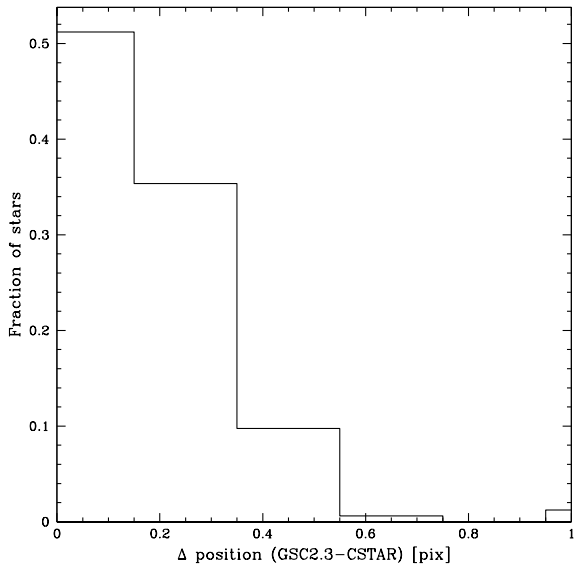

FIG. 7.— Distribution of astrometric differences between CSTAR and the Guide Star Catalog v2.3. The plate scale of CSTAR is $15''/pix$.

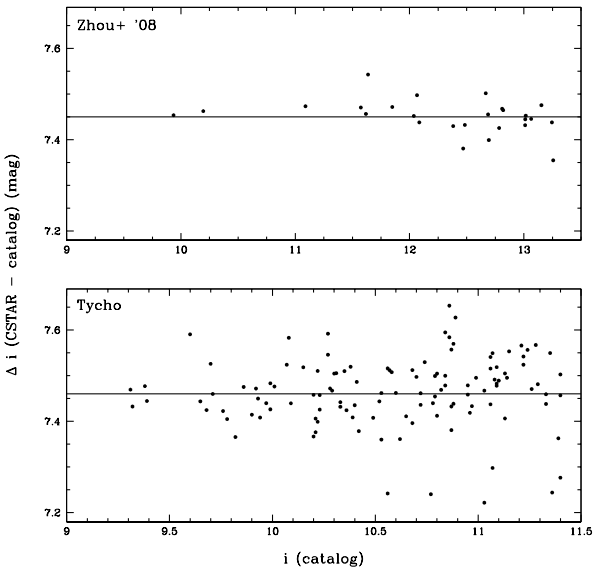

FIG. 8.— Photometric calibration of the CSTAR observations.

- Exposure time normalization: The aperture photometry reported by DAOPHOT was corrected by the usual factor of $2.5\log(t)$.

- Zeropoint correction: The zeropoint difference between each image and the photometric reference image was determined following the procedure previously described in §3

- Sigma rescaling: We rescaled the magnitude uncertainties reported by DAOPHOT so that $\chi^2_\nu = 1$ for non-variable stars, following the procedure developed by Kaluzny et al. (1998).

- Residual flat-fielding: We selected 200 bright non-variable stars and searched for correlations between their (x, y) position and deviations from their mean magnitude on every science-quality frame. We averaged the results from neighboring pixels to increase S/N, at the cost of decreasing the spatial resolution by $4\times$. The result is equivalent to a residual flat-field frame, which exhibited peak-to-peak variations of 1%.

- Time calibration: The clock in the data acquisition computer exhibited a small drift during the observing season. We corrected the Julian Dates of all science-quality frames following §4.3 of Zhou et al. (2010a).

- Masking of satellite trails: Numerous satellite trails are present in the CSTAR images, easily identifiable as lines with fluxes $> 10\sigma$ above background. This polluted stars whose positions on the CCD overlapped the trails. We used a parallelogram mask with the trail line as the bisector and a width that encompassed all pixels with fluxes $> 3\sigma$ above background. This was equivalent to a width of 20 pixels or less, depending on the brightness of each trial. We rejected the individual photometric measurements of stars lying inside the masked regions of a given frame.

- Masking of saturated regions: We masked pixels with values above 25,000 ADU and their associated bleed trails.

- Spike filtering: We detected quasi-periodic, short-duration (typically 30 min) increases in the brightness of some stars (typically 0.4 mag) which were otherwise not variable. Some of these "spikes" were due to ghosts (multiple reflections of incoming photons) of bright stars which we identified by subtracting neighboring images. We initially identified spikes by searching for 3σ deviations from the mean magnitude in 6-hour blocks of data. In the case of periodic variable stars, the mean was computed over $\frac{1}{8}$ of the period or 0.1 day, whichever was smaller. We carried out the procedure twice, shifting the starting time of each bin by half of its width on the second pass. This algorithm might have eliminated some *bona fide* aperiodic flux variations (such as stellar flares), but we defer a thorough analysis of such events and other causes of these spikes to a future publication.

- Magnitude calibration: We placed our corrected instrumental magnitudes on the standard system as described previously in §3.2.

4.2. *Photometric Precision*

Over 70% of the bright-star sample considered in this analysis have more than 20,000 photometric measurements. Thanks to this, the internal statistical uncertainty in the mean magnitudes of stars with $i \leq 13.5$ mag is less than 10^{-3} mag, as seen in Fig. 9. As discussed previously in §3.2, the *absolute* uncertainty of the photometry is limited by the synthetic magnitude calibration using the Tycho catalog.

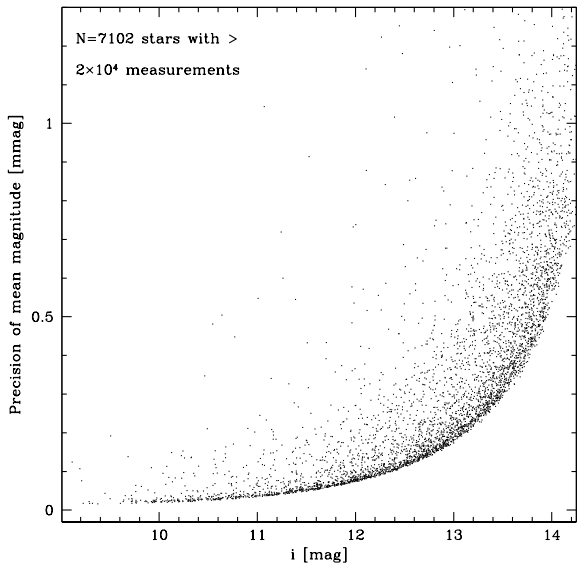

FIG. 9.— Photometric precision of mean i magnitudes for more than 7000 stars that have at least 20,000 observations.

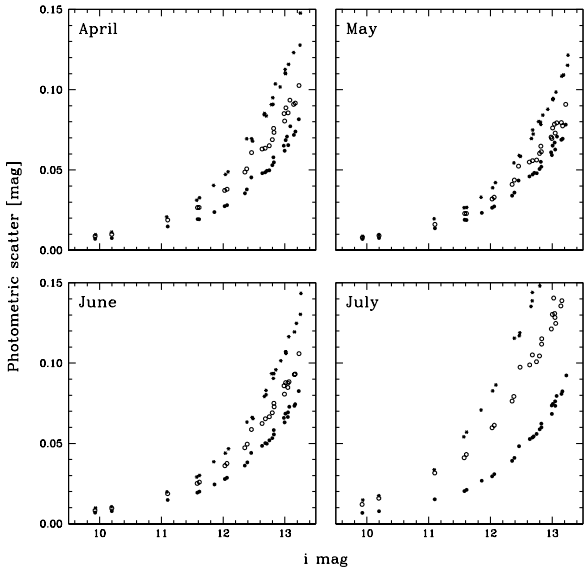

FIG. 10.— Comparison of photometric scatter for stars in common with Zhou et al. (2010a) that were used to determine the zeropoint offset in the top panel of Fig. 8. Separate comparisons are show for April, May, June and July. Starred symbols: photometry from Zhou et al. (2010a); open symbols: our aperture photometry before applying the photometric corrections described in §4.1; filled symbols: our aperture photometry after applying the corrections.

Fig. 10 compares the scatter in our mean magnitudes with the results of Zhou et al. (2010a). We compared 27 stars in common between our catalogs which were used to obtain the alternative zeropoint discussed in §3.2. We calculated the scatter in the mean magnitude of each star in both data sets using a 3σ iterative outlier rejection, performing separate comparisons for each month of the observing season. Our mean magnitudes exhibit a slightly smaller scatter than Zhou et al. (2010a). Some possible reasons for the reduced scatter include the use of a smaller sky annulus located closer to each star and the rejection of measurements affected by satellite trails.

5. VARIABLE STAR CATALOG AND STATISTICS

5.1. *Search for Variability*

We applied several techniques to quantify the variability of the bright-star sample. First, we computed the Welch-Stetson variability index L (§2 of Stetson 1996), which measures the time-dependent correlation of magnitude residuals of pairs of close observations, rescaling them according to the estimated standard error of each magnitude measurement. Fig. 11 shows the distribution of L values as a function of magnitude for this subsample.

We searched for periodic variability among the bright-star sample using three techniques. The first technique is the Lomb-Scargle method (Lomb 1976; Scargle 1982, hereafter LS), which applies the statistical properties of least-squares frequency analysis of unequally spaced data on a series of test periods. We searched for periods between 0.1 and 50 d and used a bin size of 0.01 d. Periods with $S/N \geq 10$ in the periodogram were considered to be significant. The second technique involves Fourier decomposition as implemented by the Period04 program (Lenz & Breger 2005), which is described in detail in § 5.2. We searched for frequencies between 0 and 50 cycles/day with a bin size set by the Nyquist sampling. Frequencies with $S/N \geq 4$ were considered significant.

Lastly, we searched for periodic transit events on prewhitened light curves using the box fitting algorithm (Kovács et al. 2002, hereafter BLS). This algorithm looks for signals characterized by a periodic alternation between two discrete levels with much less time spent at the low-level (occultation) phase. The duration of a transit was allowed to range between 0.01 and 0.1 of the primary period. The BLS transit period was sought over the same time span as the LS period using 10,000 trial periods and 200 phase bins. We prewhitened the selected light curves based on the most significant period ($1/f$) and its 10 higher-harmonics (frequencies of $2f$, $3f, \ldots, 11f$) and 9 sub-harmonics (frequencies of $f/2$, $f/3, \ldots, f/10$)

We found 115 periodic variables by the LS method, 29 additional periodic variables via the Fourier decomposition technique, and 10 transit events through the BLS method, for a total of 154 periodic variables.

We phased the light curves of these stars using the most significant period and calculated the median value for every 10^{-3} in phase. We calculated the L values for the binned phased light curves of these stars and compared the distribution to the one for 100 stars which had no significant periodicity. Each star in the latter sample was phased using all periods found in the former set, yielding $\sim 15,000$ test light curves. Fig. 12 shows a comparison of both distributions. We selected 149 out of 154 objects with $L_{ph} > 0.25$ as our final sample of periodic variables. We further included 8 variables with significant changes in magnitudes but no periodicity within our observing window (128 days). In these cases, we binned the data as a function of time every 3000s and found values of $L_{ph} > 2$ in all cases.

The final sample of 157 variable stars is presented in Table 3. Column 1 gives the CSTAR ID; column 2 gives the ID from the Guide Star Catalog, version

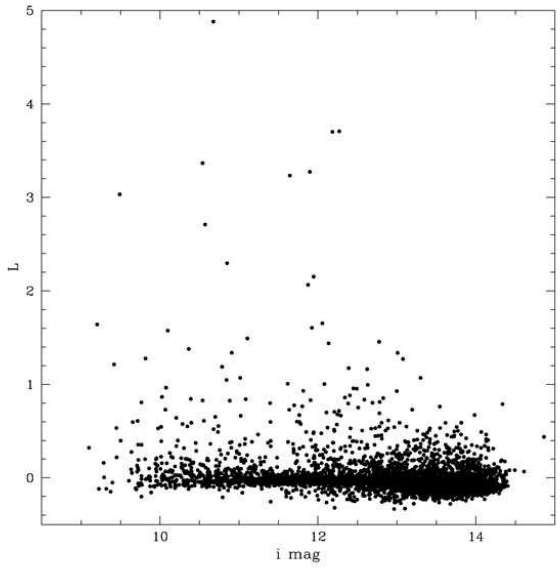

FIG. 11.— Variability statistic L (Stetson 1996) for the 10,000 brightest stars in the CSTAR sample.

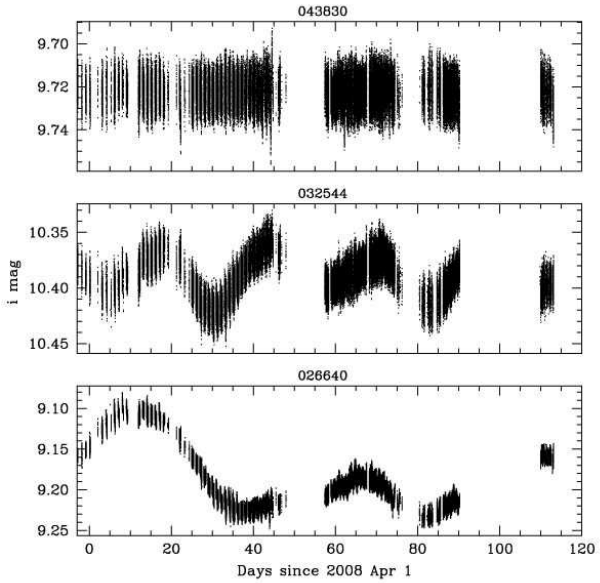

FIG. 13.— Light curves of a bright constant star (top panel) and two variable stars (bottom two panels).

2.3.2 (GSC2.3); columns 3 and 4 give the right ascension and declination from GSC2.3; column 5 gives the mean i-band magnitude; column 6 gives the main period, and column 7 gives a tentative classification of the variable type, when possible. Fig. 13 shows the time series of three bright stars (one constant and two variables). Fig. 14 shows folded light curves of a representative subset of the periodic variables, while Figs. 15a-f show the time-series light curves for another representative subset of the periodic variables. Lastly, Figs. 16a-b show two examples of variables with long-term trends but no periodicity in our observing window.

28 CSTAR variables appear in previous variable-star catalogs: the All-Sky Automated Survey (ASAS, Pojmanski 2005) and the General Catalog of Variable Stars (GCVS, Samus et al. 2009). The variables in common are listed in Table 4. The periods we derived are in good agreement with previous determinations except for CSTAR#032007, #052891 and #136863. The first two variables have CSTAR periods that are $\sim 2\times$ the ASAS values, while the last one exhibits long-term variability in the CSTAR data which does not match the ASAS period.

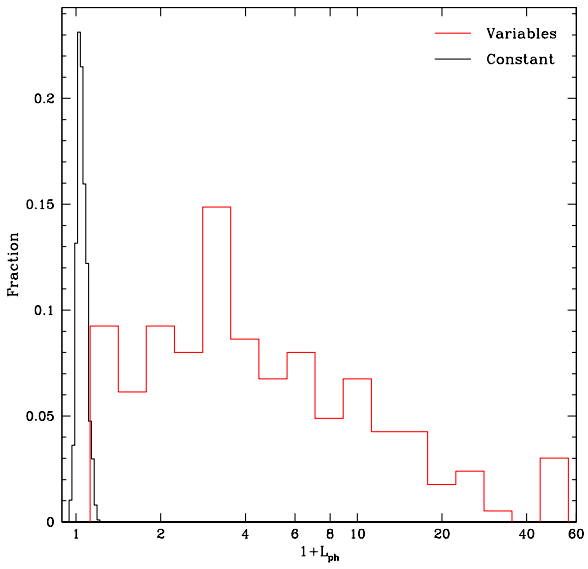

FIG. 12.— Histogram of variability statistic L for objects that exhibited a significant periodicity using the LS technique (red), compared to the equivalent distribution for objects without a significant periodicity (black). The variability statistic was computed using phased light curves with 10^3 points per cycle.

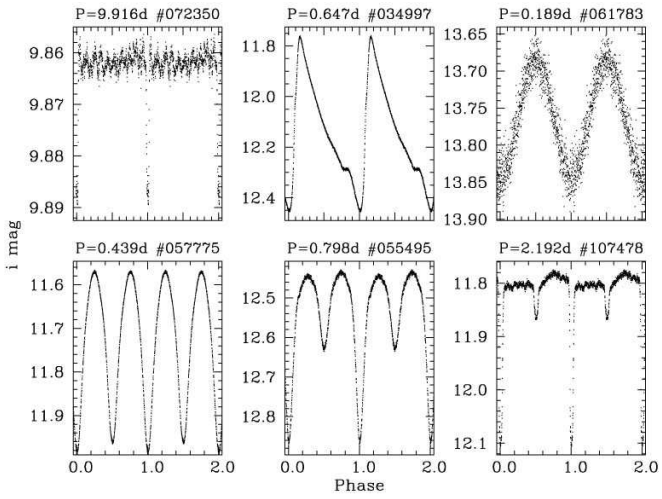

FIG. 14.— Phased light curves of six variable stars. The periods and CSTAR IDs are given in the figure. Top row, from left to right: transit variable; RR Lyrae; δ Scuti. Bottom row, from left to right: eclipsing binaries of contact (EC), semi-detached (ESD), and detached (ED) configurations.

We were unable to recover 14 previously-known variables: 12 are saturated and 2 lie very close to saturated stars and were masked in our master frame. In the magnitude range $9.18 < i < 14.15$ that we have in common with GCVS and ASAS, we found 5× more variable stars.

We classified approximately half of the variables into one of five types: binaries, δ Scuti, γ Doradus, RR Lyrae, and objects with long-term variability which may be periodic beyond our observing window. One variable exhibits a light curve consistent with an exoplanet transit. Table 5 contains crude statistics for the different types.

5.2. *Search for multiple periods via Fourier Decomposition*

We searched for multiple periods in the time-series photometry of the variables using the Period04 program (Lenz & Breger 2005). We started by identifying the frequency (f_1) that displayed the highest S/N peak in the periodogram. Next we prewhitened the time series (i.e., subtracted off the most significant frequency) and searched for the next highest peak in the frequency spectrum. We repeated the process until all peaks with $S/N > 4$ were identified. For example, consider the variable CSTAR#061353, shown in Fig. 17. There are three significant peaks in the periodogram, with $f_i = 44.2879$, 44.1690, and 42.1209 cycles d^{-1}) and signal-to-noise ratios of 15.8, 15.7, and 15.0, respectively. The top left inset shows the phased light curve for $f_1 = 44.2879$ cycles d^{-1} with 1000 phase bins. Given the amplitude-frequency plot and the phased light curve, the dominant period of 32 minutes is likely real.

The Fourier decomposition results of all the periodic variables are listed in Table A1. We list in columns 2, 3, and 4 the frequency, amplitude (in mmag), and signal-to-noise ratio of each peak. Column 5 gives the relations between the primary and other frequencies. We do not list 4 transit-like variables with $P > 6$ d(072350, 081845, 097230, 131919) for which we only have a period based on the BLS method.

5.3. *Types of variables found by CSTAR*

5.3.1. *Eclipsing binaries*

Eclipsing binaries can be classified into three broad categories (Paczyński et al. 2006): contact (EC), semi-detached (ESD) and detached (ED). Typical light curves are shown in the three bottom panels of Fig. 14 and in Figs. 15a, b and c.

There are 10 binaries among the 27 variables in common with ASAS (CSTAR#001707, 020526, 022489 036162, 038255, 038663, 055495, 057775, 083768, 133742). Their Fourier spectra show that the frequencies found are often integral or half-integral multiples of each other. We identified an additional 31 variables exhibiting similar Fourier properties and light curves.

5.3.2. *δ Scuti Stars*

δ Scuti variables are late A- and early F-type stars situated in the instability strip on or above the main sequence in the HR Diagram. Their typical pulsation periods are found to be in the interval of 0.02d to 0.25d (Breger 2000). The frequencies of 9 candidates are in the range 4 to 30 cycles d^{-1} such as star 061783 in Table A1.

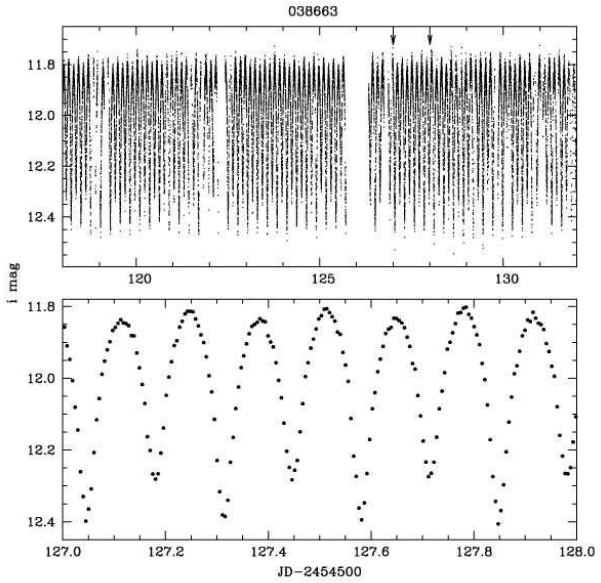

FIG. 15A.— Time-series light curve of a contact binary. Only a small fraction of the complete CSTAR data is shown. The top panel shows the light curve sampled at 20s intervals. The bottom panel shows a portion of the top light curve (bounded by the arrows) binned into 450s intervals.

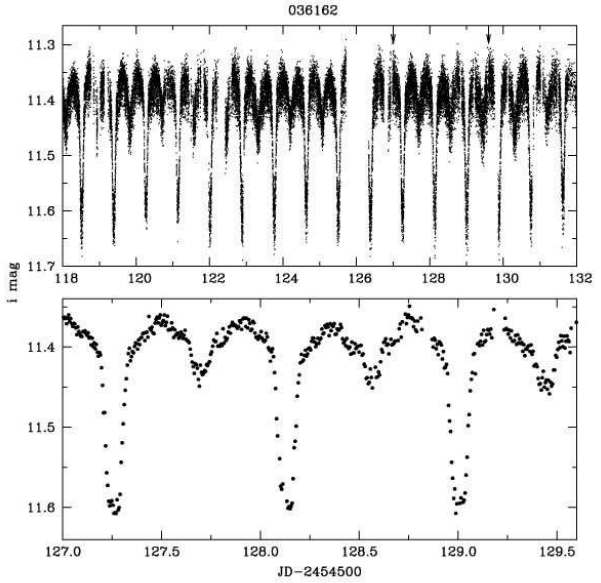

FIG. 15B.— Same as 15a, but for a semi-detached binary.

TABLE 3
Variable stars

CSTAR	ID GSC	R.A. (GSC[1])	Dec. (GSC[1])	i (mag)	Period (d)	Src[2]	T_0^3 (d)	Type[4]
000572	S3YM000353	11:11:19.60	−87:18:00.9	13.88	0.154415	LS	55.3409	DSCT
001707	S74D000321	12:32:42.91	−87:26:22.9	11.07	0.338528	LS	56.5058	EC, [A]
003125	S3YM000469	10:43:46.63	−87:25:10.1	9.68	3.586394	LS	...	Binary?
003697	S742000061	12:08:11.93	−87:35:39.9	11.55	26.065850	LS	...	
003850	S742000043	12:34:25.12	−87:34:37.7	10.14	14.928409	P04	...	[A]
004463	S3YM000518	10:40:16.05	−87:29:29.8	11.16	0.434167	LS	55.5901	Binary?
005954	S742000078	12:39:58.23	−87:41:37.2	11.68	74.844696	P04	...	
008426	S3YM000629	10:14:50.45	−87:36:23.8	11.10	8.768682	LS	...	
009171	S3YM000662	10:12:54.85	−87:38:22.9	13.95	0.591609	LS	55.9779	RRL, [A]
009952	S742000182	12:43:30.67	−87:53:30.9	11.39	23.675364	P04	...	[A]
011616	S3Y9000240	10:56:28.86	−87:55:21.0	11.97	30.935810	LS	...	
011709	S742000246	12:41:44.27	−87:58:28.5	11.40	2.950398	LS	58.0466	EC
011796	S742000286	12:21:35.82	−88:00:14.5	12.20	1.893822	LS	56.5289	ESD
013140	S3Y9000236	10:25:53.99	−87:53:40.8	9.81	20.532616	P04	...	
013255	S74F000377	14:54:21.37	−87:21:05.0	9.84	...	...	...	LT, [A]
013432	S3YN000438	09:10:17.59	−87:24:06.0	11.46	74.811104	P04	...	
014111	S74F000634	14:29:01.63	−87:38:16.2	13.68	0.174075	LS	55.4082	EC
014368	S3YM000753	10:03:10.79	−87:51:06.2	10.77	...	...	...	LT
014495	S3Y9000339	10:49:00.65	−88:02:17.2	12.24	18.711236	LS	...	
016836	S742030458	12:49:16.22	−88:11:17.6	13.70	0.176211	LS	55.3351	EC
018708	S3YN000609	09:02:20.82	−87:37:41.0	12.38	1.627682	LS	56.1166	Binary?
020436	S3YN000517	08:40:33.28	−87:28:38.6	12.55	55.208965	P04	...	
020526	S742000504	13:23:49.26	−88:16:04.3	12.41	2.510798	LS	56.6054	ESD, [A]
022489	S3Y9000527	10:01:21.80	−88:13:30.8	11.88	0.652255	LS	55.8390	EC, [A]
023614	S742000638	12:09:34.38	−88:29:59.0	11.49	...	...	...	LT
023885	S742000650	12:01:19.22	−88:30:46.1	11.17	1.737463	LS	...	
025440	S742000656	12:12:56.28	−88:34:11.6	10.78	9.823067	LS	...	
025846	S742000671	14:25:39.12	−88:14:54.1	13.76	9.781566	LS	...	
026640	S3YB000429	11:17:00.40	−88:35:36.4	9.19	49.365707	P04	...	[A]
026730	S3YB000202	09:58:36.02	−88:23:59.9	12.89	2.065619	LS	56.9905	ED
027082	S743000019	13:19:17.39	−88:33:00.7	11.22	6.632957	LS	...	
027575	S743000159	14:31:54.23	−88:17:39.3	10.60	6.157666	LS	...	
028221	S3YB000436	11:04:06.48	−88:38:02.5	13.56	4.843837	LS	...	
029379	S74E000029	15:57:05.68	−87:30:05.4	11.95	3.102692	LS	...	CW-FO/EC, [A]
030353	S3YA000615	08:39:40.45	−88:03:19.4	12.92	1.046833	LS	56.3738	
032007	S3YB000225	09:29:39.14	−88:30:06.4	11.77	0.621936	LS	56.0565	RRL, [A], [G]
032544	S3Y8000312	11:48:09.42	−88:49:52.6	10.39	52.022440	LS	89.0185	
034389	S3YB006313	09:49:58.18	−88:41:27.2	14.04	1.735374	LS	...	
034669	S743000094	13:50:03.38	−88:46:13.2	10.06	14.610884	LS	...	
034724	S3YB000482	10:01:18.94	−88:44:36.8	10.07	42.966682	LS	...	DCEP-FU, [A]
034997	S743000311	14:29:04.38	−88:38:43.7	12.08	0.646586	LS	55.6868	RRL, [A]
035468	S3YA000613	08:08:46.28	−88:00:02.0	13.81	0.822906	BLS	56.1514	ED?
036162	S3YB000243	09:03:59.29	−88:33:07.6	11.40	0.873470	LS	55.6252	ESD, [A]
036508	S74E000310	16:32:13.29	−87:16:17.0	13.02	37.533190	LS	...	
036526	S743000153	15:35:01.14	−88:16:11.9	12.30	...	...	...	LT
036939	S743000200	15:25:11.74	−88:23:14.9	12.82	7.384502	LS	...	
037016	S743000186	15:28:41.36	−88:21:44.0	13.60	0.157944	LS	55.3402	DSCT
037271	S740000037	12:42:14.25	−88:59:05.0	12.55	13.123393	LS	...	
038255	S743000115	13:53:18.49	−88:54:14.6	12.81	0.266903	LS	55.5067	EC, [A]
038580	S3Y8000346	10:50:11.96	−88:59:54.1	11.76	6.967593	LS	...	
038663	S3YB000253	08:46:12.64	−88:33:42.9	11.96	0.267127	LS	55.4568	EC, [A]
039541	S740000060	12:36:24.67	−89:04:02.7	10.97	13.745355	LS	...	
040351	S3YA000660	08:02:26.52	−88:14:26.1	13.33	0.285578	LS	55.4676	DSCT
042081	S743000391	14:51:21.48	−88:51:53.5	12.34	6.281005	LS	...	
042266	S3YL000384	07:16:52.61	−87:28:56.4	13.66	0.383158	LS	57.3796	EC
043618	S3YB009826	08:40:28.89	−88:47:00.4	13.69	12.998266	LS	65.4350	ESD
043885	S3YB000275	08:17:16.96	−88:37:29.5	13.90	9.439374	LS	...	
044751	S740000101	13:01:29.04	−89:13:47.0	13.18	6.495565	LS	...	
047176	S3YA000181	07:12:14.54	−87:51:19.7	12.79	2.626902	LS	...	Binary?
048452	S3YB000382	08:21:18.73	−88:55:48.2	13.40	9.975068	LS	...	
048615	S743000407	15:44:38.97	−88:54:18.9	13.44	2.919245	LS	...	
050375	S3YB013754	07:39:17.11	−88:40:41.7	13.45	1.440770	LS	56.6100	
050773	S74E000469	17:10:42.44	−87:30:09.3	10.55	3.265063	LS	...	Binary?
052891	S741000155	17:13:18.69	−87:42:28.6	9.50	53.957802	P04	...	MISC/SR, [A]
053446	S3Y8000220	08:05:03.24	−89:07:54.3	12.95	1.071097	LS	55.9342	Binary?
053570	S743000460	16:44:10.40	−88:38:19.9	11.02	19.238876	LS	...	
053783	S3Y8000272	09:44:14.75	−89:28:17.6	10.48	16.620420	LS	...	Binary?
055495	S3Y8000078	07:43:54.49	−89:07:37.3	12.51	0.797670	LS	55.7331	ESD, [A]
055854	S3Y8000109	07:54:37.65	−89:15:40.9	9.76	58.004639	P04	...	
057247	S741000463	17:18:35.08	−88:12:47.1	13.45	42.032624	LS	...	
057344	S741000539	17:13:42.52	−88:24:52.5	11.08	20.533037	P04	...	
057775	S3YA000492	06:40:47.15	−88:15:21.3	11.70	0.438611	LS	55.5992	EC, [A]
059811	S3YA000336	06:28:42.76	−88:02:41.7	12.36	7.259171	BLS	62.4178	ED
061353	S740000342	17:15:45.51	−89:00:42.8	10.78	0.022581	P04	55.2804	

TABLE 3 — *Continued*

CSTAR	ID GSC	R.A. (GSC[1])	Dec. (GSC[1])	i (mag)	Period (d)	Src[2]	T_0^3 (d)	Type[4]
061658	S741000489	17:36:45.98	−88:14:10.5	11.31	0.076167	BLS	55.3337	DSCT
061740	S740000322	17:23:25.05	−88:53:37.3	9.97	25.220045	P04	...	
061783	S740000308	17:25:37.17	−88:49:50.3	13.74	0.188991	LS	55.4105	DSCT
062683	S3Y8000165	07:46:18.25	−89:40:00.7	10.27	22.526073	P04	...	
062854	S3YA000596	06:23:15.53	−88:33:35.4	12.68	34.733614	LS	...	
063059	S3Y8000125	06:49:54.20	−89:21:58.8	9.44	15.164152	P04	...	
063241	S3YA000025	06:12:09.29	−87:27:15.6	13.81	0.131663	LS	...	DSCT
064380	S3YA000248	06:10:28.12	−87:53:32.9	14.14	2.309535	LS	...	
064944	S741000460	17:51:13.16	−88:09:48.8	10.63	12.420856	LS	...	
065072	S740000301	17:47:26.35	−88:46:07.9	11.87	0.620578	LS	55.4131	
066196	S740000469	17:05:16.14	−89:51:43.8	9.65	45.493835	P04	...	
066682	S3YA021353	06:03:05.44	−88:29:29.3	13.43	1.272036	LS	...	
066775	S741000378	17:59:00.73	−88:01:32.9	11.76	27.296301	P04	...	
068276	SA9S000144	18:22:33.29	−89:36:22.9	11.40	2.796789	LS	55.2942	Binary?
068308	S0SG000353	05:50:34.20	−89:06:46.2	12.93	0.798475	LS	...	
068493	S0SH000282	05:55:30.36	−87:57:06.8	14.02	0.714096	BLS	...	
068908	SA9U000383	18:08:15.09	−88:18:02.9	10.83	2.645011	LS	...	
069430	S0SH026837	05:48:54.94	−88:30:16.6	14.02	13.380021	LS	...	
070680	SA9S000413	22:05:02.55	−89:52:06.7	13.01	1.987754	LS	55.9380	ESD
070941	S0SH000215	05:47:08.05	−87:51:00.2	10.22	0.606466	LS	55.7721	GDOR
071571	S0SH000333	05:43:19.93	−88:04:04.3	10.57	...	...	...	LT, [A]
072350	SA9V000050	18:30:57.87	−88:43:17.5	9.86	9.916101	BLS	63.6590	transit
072730	SA9U000438	18:29:03.93	−88:32:31.9	13.26	0.573063	LS	55.7163	RRL, [A]
073028	S0SH000497	05:30:59.30	−88:30:04.7	13.52	9.675598	LS	...	
073846	SA9U000442	18:35:37.14	−88:33:45.9	11.97	12.501163	LS	...	
076135	SA9S000115	19:53:21.15	−89:22:46.5	10.49	...	...	...	LT
076723	SA9V000063	19:00:22.60	−88:47:53.7	10.84	51.559681	P04	...	
077171	SA9S015549	23:03:19.23	−89:39:40.4	10.10	5.681234	LS	...	
077190	S0SH000448	05:15:49.62	−88:17:51.5	10.20	49.365650	P04	...	
077508	SA9S000404	22:53:06.46	−89:38:40.9	14.04	0.133311	LS	55.4247	DSCT
077594	SA9V000067	19:08:12.87	−88:49:18.5	10.06	1.677415	LS	56.7822	
078549	S0SH000321	05:15:49.03	−88:04:23.5	13.10	5.393342	LS	65.7215	EC?
078773	SA9V000073	19:17:53.08	−88:51:11.2	11.81	0.186027	LS	55.2921	EC
079397	SA9S000068	19:48:57.10	−89:07:14.3	10.86	4.851947	LS	...	
080934	SA9U000331	18:58:35.51	−88:12:55.2	11.74	64.449600	P04	...	
081428	S0SG000131	00:46:05.01	−89:31:34.7	10.38	10.643167	P04	...	
081563	SA9V000069	19:33:28.81	−88:48:44.8	12.77	23.342061	LS	...	
081723	SA9U000071	18:48:23.75	−87:43:16.4	11.48	0.841544	LS	56.0909	GDOR
081749	...	19:11:53.61	−88:27:14.9	10.30	70.308655	P04	...	
081845	SA9V000074	19:38:27.80	−88:50:55.9	12.89	6.767879	BLS	56.0302	ED?
082180	S0SG000129	00:29:58.19	−89:30:20.3	11.24	0.152807	LS	55.3621	EC?
082489	S0SG000205	03:11:22.58	−89:15:13.6	14.08	0.172334	LS	55.6132	EC
083110	S0SG000226	02:11:02.80	−89:22:50.3	10.27	40.003201	P04	...	
083768	S0SU000304	05:13:29.62	−87:19:42.6	12.04	0.384076	LS	55.5749	EC, [A]
084344	SA9S000371	23:01:30.03	−89:25:01.5	13.94	1.466449	LS	...	
085531	SA9U000338	19:20:09.67	−88:14:03.9	13.66	6.367062	LS	...	
085719	S0SG000178	03:08:19.12	−89:06:32.2	12.19	16.573029	P04	...	
086480	S0SJ000306	03:44:10.88	−88:52:09.5	11.19	23.017941	LS	...	
087084	SA9S000168	20:57:31.47	−89:03:50.3	12.39	1.857031	BLS	56.6568	ED?
087501	S0SG000092	01:23:01.27	−89:17:09.4	13.54	0.193486	LS	55.3480	EC?
087548	S0SH000485	04:20:11.85	−88:25:03.5	12.62	0.197741	LS	55.3917	EC
088142	S0SG000093	00:52:40.76	−89:17:32.4	13.75	0.292953	LS	55.3454	EC
089391	SA9U000387	19:43:40.77	−88:19:20.7	13.48	0.136882	LS	...	
093873	SA9S000300	22:17:44.44	−89:01:38.1	9.42	34.120377	P04	...	
094793	S0SU000407	04:36:31.02	−87:28:03.3	10.96	0.616082	LS	...	
096404	SAA5000420	19:43:05.07	−87:46:52.4	13.93	0.581793	LS	55.9001	RRL, [A]
097230	SA9U000295	20:02:18.84	−88:02:50.0	12.06	19.253283	BLS	66.7927	ED?
097790	SA9V000415	22:23:40.80	−88:53:42.9	9.71	0.521650	LS	55.4856	GDOR
098092	S0SH000022	03:54:41.13	−88:02:50.6	11.63	89.237907	P04	...	[A]
098719	SAA5000417	19:50:26.13	−87:44:50.7	12.80	0.208220	LS	55.3070	EC
099529	S0SG000018	00:31:15.83	−88:55:17.9	10.79	4.833741	LS	...	
106019	S0SU000388	04:02:44.72	−87:22:26.5	10.60	32.131606	LS	...	
106769	SA9V000337	22:04:27.19	−88:29:34.7	13.66	24.117975	LS	...	
107478	SAA5000503	20:28:30.07	−87:46:16.5	11.80	2.192167	LS	55.7692	ED/ESD
110801	S0SI000269	02:42:27.87	−88:04:22.5	9.48	35.695164	P04	...	[A]
111298	S0SI000438	02:12:56.05	−88:13:52.5	10.01	11.922923	LS	...	
113453	S0SI000393	00:45:26.78	−88:25:21.3	11.57	34.526609	LS	...	
114506	S0SV000507	02:55:24.43	−87:48:18.6	12.09	3.852912	BLS	57.4873	
116410	S0SV000502	02:47:02.44	−87:47:06.9	11.60	3.693423	LS	...	
116471	S0SV000340	03:22:43.36	−87:23:34.4	13.44	0.263255	LS	...	DSCT?
117654	S0ST000503	02:18:11.67	−87:56:11.2	10.54	21.683977	P04	...	
118705	S0SI033411	00:53:26.68	−88:12:41.4	13.37	8.461614	LS	...	
119488	S0SI000329	00:08:43.43	−88:13:48.4	10.07	80.006401	P04	...	
120188	S0SI000289	00:55:45.92	−88:09:11.0	11.16	10.711880	LS	...	
121369	SA9T000310	23:15:35.46	−88:07:33.8	10.77	21.092596	P04	...	

TABLE 3 — *Continued*

CSTAR	ID GSC	R.A. (GSC[1])	Dec. (GSC[1])	i (mag)	Period (d)	Src[2]	T_0^3 (d)	Type[4]
121389	S0SV000324	03:02:08.67	−87:22:53.3	13.73	44.773727	LS	...	
123934	SA9T000282	23:52:30.36	−88:03:49.5	13.91	0.122021	LS	...	DSCT?
124666	SAA6000034	21:47:16.29	−87:39:06.6	12.75	0.458038	LS	55.5358	RRL, [A]
127850	S0SI014387	00:00:52.46	−87:54:27.3	11.79	...	...	...	LT, [G]
128178	S0SI000097	01:08:04.79	−87:47:59.1	13.87	15.846209	LS	...	
131919	S0SI000101	00:01:16.84	−87:44:02.9	11.97	9.448529	BLS	57.2732	ED
133742	SAA6000366	22:37:07.30	−87:28:49.9	11.58	0.848378	LS	55.9822	EC, [A]
136863	SAA6000283	23:01:23.88	−87:22:19.9	9.50	...	...	...	LT, [A]

NOTE. — [1]: if the star is not in GSC2.3, the position is based on the CSTAR master image. [2] Source of period: [LS], Lomb-Scargle method; [BLS], box fitting algorithm; [P04], Fourier decomposition with Period04 program. [3] Epoch of primary eclipse or minimum light (when applicable), in JD-2454500. [4] Type: [A], ASAS variable; [G], GCVS variable; CW-FO, W Virginis variable, first-overtone pulsator; DCEP-FU, δ Cephei variable, fundamental-mode pulsator; DSCT, δ Scuti variable; EC, contact binary; ESD, semi-detached binary; ED, detached binary; GDOR, γ Doradus variable; LT, long-term trend; MISC/SR, Miscellaneous/semi-regular variable; RRL, RR Lyrae variable.

TABLE 4
VARIABLES IN COMMON BETWEEN CSTAR AND OTHER CATALOGS

CSTAR	ID Other	P (d) CSTAR	P (d) Other
001707	[A]123244-8726.4	0.338528	0.338519
003850	[A]123423-8734.6	14.928409	18.63354
009171	[A]101257-8738.4	0.591609	0.59161
009952	[A]124330-8753.5	23.675364	23.71541
013255	[A]145422-8721.1	LT	174.6807
020526	[A]132341-8816.1	2.510798	2.51046
022489	[A]100123-8813.5	0.652255	0.65226
026640	[A]111701-8835.6	49.365707	51.8
029379	[A]155703-8730.1	3.102692	3.115622
032007	[A]092907-8829.7	0.621936	0.38355
034724	[A]100112-8844.6	42.966682	43.5
034997	[A]142904-8838.7	0.646586	0.64655
036162	[A]090354-8833.1	0.873470	0.87376
038255	[A]135318-8854.2	0.266903	0.266899
038663	[A]084613-8833.7	0.267127	0.267128
052891	[A]171319-8742.5	53.957802	29.036005
055495	[A]074400-8907.7	0.797670	0.79801
057775	[A]064047-8815.4	0.438611	0.43863
071571	[A]054317-8804.1	LT	426
072730	[A]182912-8832.6	0.573063	0.573034
083768	[A]051332-8719.7	0.384076	0.38408
096404	[A]194301-8746.9	0.581793	0.58171
098092	[A]035443-8802.8	89.237907	70.7
110801	[A]024230-8804.4	35.695164	47.6
124666	[A]214719-8739.1	0.458038	0.45803
127850	[G] ST Oct	LT	LT
133742	[A]223703-8728.8	0.848378	0.84838
136863	[A]230125-8722.3	LT	37.31343

NOTE. — [A]: ASAS; [G]: GCVS; LT=long-term variability.

TABLE 5
DISTRIBUTION OF VARIABLE STAR TYPES

Variable Type	N	%
Binary	41	26.1
δ Sct	9	5.7
Long-term	8	5.1
RR Lyr	6	3.8
γ Dor	3	1.9
Transit	1	0.6
Unclassified	89	56.7

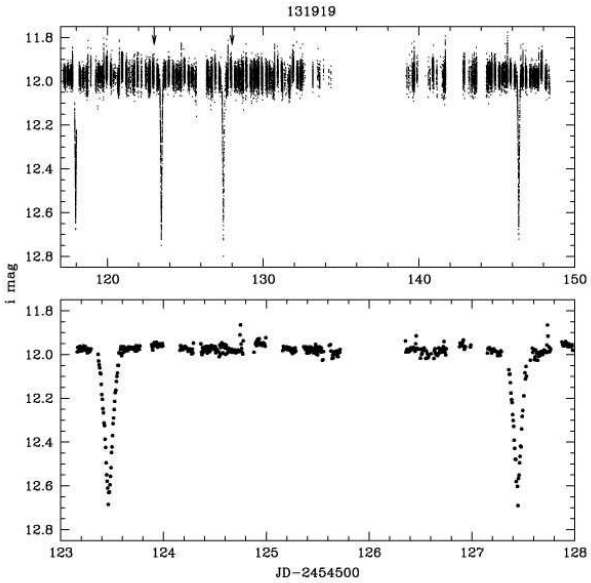

FIG. 15c.— Same as 15a, but for a detached binary.

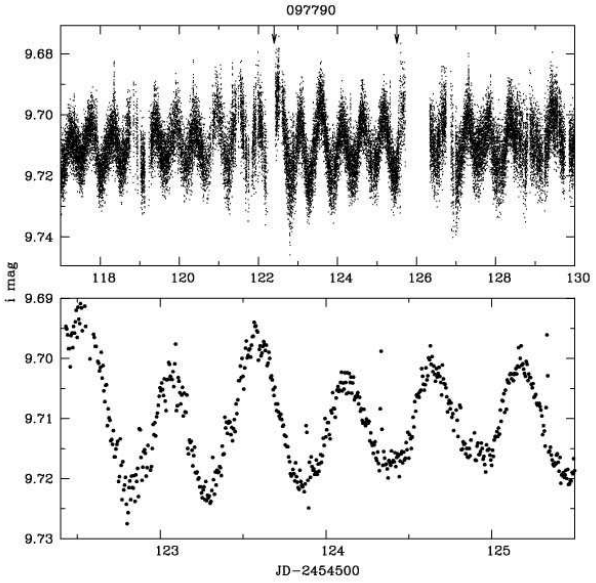

FIG. 15d.— Same as 15a, but for a variable of γ Dor type.

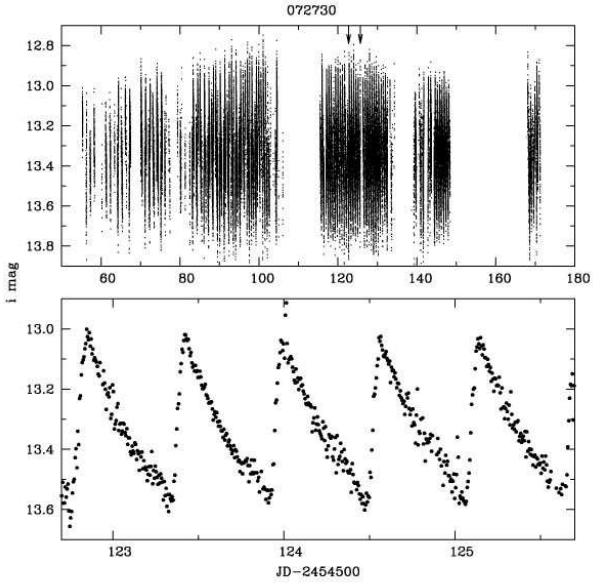

FIG. 15E.— Same as 15a, but for a variable of RR Lyr type with Blazhko effect.

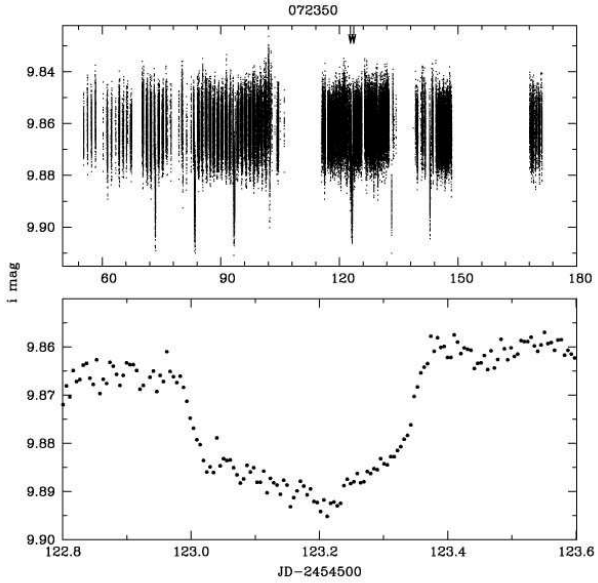

FIG. 15F.— Same as 15a, but for a possible transiting exoplanet.

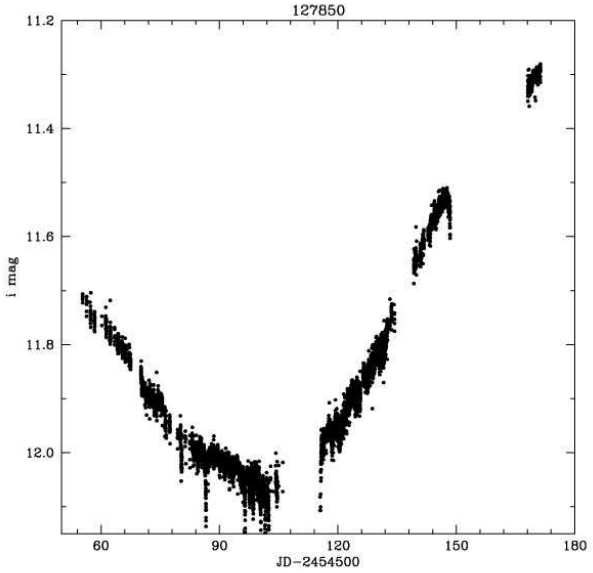

FIG. 16A.— Complete CSTAR light curve for a long-term variable, binned at 450s intervals.

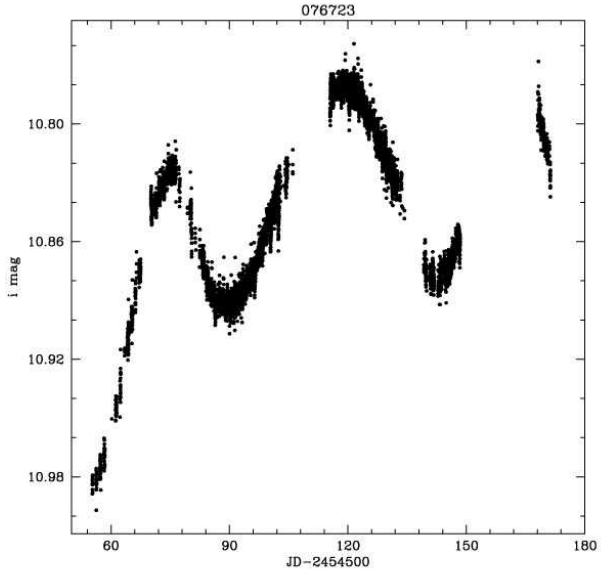

FIG. 16B.— Complete CSTAR light curve for a long-term variable, binned at 450s intervals.

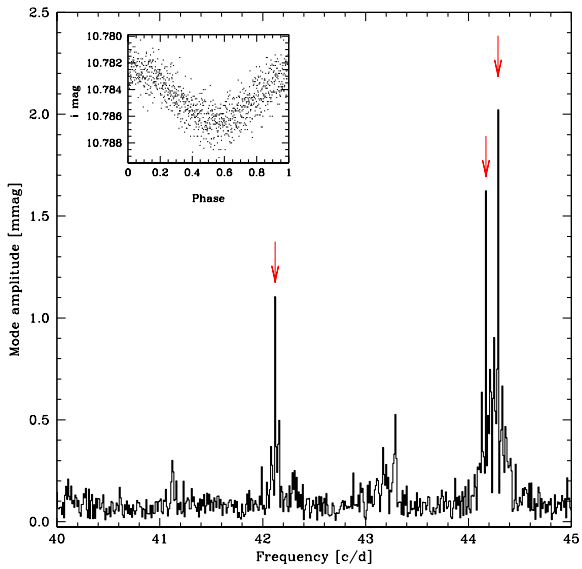

FIG. 17.— Fourier spectrum of variable candidate ID = 061353 derived using the Period04 program. There are three significant peaks, at f_i = 44.288, 44.169, and 42.121 cycles d^{-1}. The inset on the top-left corner shows the light curve phased using f_i=44.288 cycles d^{-1}. See Table A1 for details.

5.3.3. *γ Doradus Stars*

γ Doradus variables constitute a class of multi-periodic pulsating variables that have a strong asteroseismic potential since they are located in a region of the HR Diagram where g-mode pulsations, p-mode pulsations and solar-like variability may exist in a single star (Kaye et al. 1999). They are of spectral type A or F and are located on or just above the main sequence. Observationally, they exhibit multiple periods between 0.3 and 3 d, with typical photometric amplitudes of 5 to 50 mmag (Cuypers et al. 2009). Based on the Fourier decomposition, three candidates are likely γ Dor stars. Star 070941 has three frequencies of 1.65, 1.60, and 1.83 cycles d^{-1}. Its spectral type is F0 from the Tycho-2 Spectral Type Catalog (Wright et al. 2003). It is located at RA = 05:47:08.050, DEC:−87:51:00.17 (J2000). To our knowledge there are no published spectra of the other two candidates (081723, and 097790 shown in Fig. 15d).

5.3.4. *RR Lyrae Stars*

RR Lyrae are low-mass stars undergoing helium core fusion with spectral types ranging from A2 to F6 (Smith 1995). They exhibit periods from ~ 0.2 to ~ 1 day and photometric amplitudes in the optical bands of 0.3 to 2 mag. Most RR Lyrae stars pulsate in the radial fundamental mode (RRab stars). RRc stars pulsate radially in the first overtone. RRd stars, which are much rarer, pulsate in both modes simultaneously. There are six RRAB stars in our sample (009171, 032007, 034997, 072730, 096404, 124666), all of which were previously identified by ASAS. Additionally, CSTAR#032007 is listed in the GCVS as W Oct.

Some RR Lyrae stars show modulations in their period, pulsation amplitude, light curve shape, and radial velocity curves. These modulations are known as the "Blazhko effect" (Blažko 1907; Buchler & Kolláth 2011). Previous surveys have found different percentages of RR Lyrae exhibiting the Blazhko effect: 10-30% of RRab variables in Alcock et al. (2003), and 50% in Jurcsik et al. (2009). The Fourier spectrum of a Blazhko-effect RRLyrae is characterized by triplets, quintuplets and high-order multiplets around the pulsation frequency components.

Based on the period analysis in Table A1 and light curve shapes we found 4 out of 6 RR Lyr stars in our sample exhibit the Blazhko effect (034997, 072730, 124666, 032007). One such star is shown in Fig. 15e.

5.3.5. *Other Types of Variables*

Variable CSTAR#072350 displays a transit-like light curve with a period of 9.916d and a depth of 17 mmag, shown in the top left panel of Fig. 14 and Fig. 15f. The primary is a bright F5 star with $T_{\rm eff} \sim 6400$ K from the Tycho-2 Spectral Type Catalog (Wright et al. 2003). If confirmed, this would be an interesting addition to the known extrasolar planets given the relatively long orbital period and temperature of the primary.

There are 8 variable candidates with long-term trends, which may have periods longer than the observing window of 128 d. Some are probably Mira stars, such as CSTAR#127850 which shows an amplitude variation of 1.4 mag. Its light curve is plotted in Fig. 16a.

89 variable candidates have no classification in column 6 of Table 3; half of these were previously unknown. Follow-up photometric and spectroscopic observations will be required to determine their nature. One of these variables, CSTAR#065072, has been spectroscopically identified as a M3.5 dwarf in the solar neighborhood by Riaz et al. (2006).

5.4. *Blending*

The large pixel scale of the camera and the relatively high stellar density of the field makes blending a problem. We define a blend as two or more stars located within 30 arcseconds ($\sim$ 2 CSTAR pixels) of each other. Inspection of DSS images reveals that $\sim 1/3$ of the candidate variable stars are blended with one neighboring star while $\sim$ 6% are blended with two or more neighboring stars. Follow-up photometry with a finer pixel scale will be required to ensure these blends are not responsible for the observed variability. Future telescopes planned for Dome A will yield a considerably finer pixel scale which will mitigate this problem (AST3, Cui et al. 2008). Additionally, we are implementing a difference-imaging photometry pipeline that will enable a more robust detection of variables in crowded environments and will deliver higher photometric precision.

6. SUMMARY

CSTAR has a large field of view (23 square degrees) and the ability to provide uninterrupted observations for the entire duration of the Antarctic winter night. We have obtained high-quality time-series photometry for 10,000 stars with $i < 14.5$ mag and detected 157 variables, 5× more than previous surveys of same area of the sky in the same magnitude range.

Our photometry indicates that Dome A is a viable and excellent observing site. During the 2008 Antarctic winter season, 96% of the images obtained at a solar ele-

vation angle below -10° were useful for scientific purposes. The median sky background in the i band was 19.6 mag/$\Box''$ and the median extinction due to clouds was below 0.1 mag.

Lingzhi Wang acknowledges financial support by the China Scholarship Council and the National Natural Science Foundation of China under the Distinguished Young Scholar Grant 10825313 and Grant 11073005, by the Ministry of Science and Technology National Basic Science Program (Project 973) under grant number 2007CB815401, and by the Excellent Doctoral Dissertation of Beijing Normal University Engagement Fund.

Lucas Macri and Lifan Wang acknowledge support by the Department of Physics & Astronomy at Texas A&M University through faculty startup funds and the Mitchell-Munnerlyn-Heep Chair for tenure-track faculty.

This work was supported by the Chinese PANDA International Polar Year project, NSFC-CAS joint key program through grant number 10778706, CAS main direction program through grant number KJCX2-YW-T08. The authors deeply appreciate the great efforts made by the 24-27th Dome A expedition teams who provided invaluable assistance to the astronomers that set up and maintained the CSTAR telescope and the PLATO system. PLATO was supported by the Australian Research Council and the Australian Antarctic Division. Iridium communications were provided by the US National Science Foundation and the US Antarctic Program.

REFERENCES

Alcock, C., Alves, D. R., Becker, A., Bennett, D., Cook, K. H., Drake, A., Freeman, K., Geha, M., Griest, K., Kovács, G., Lehner, M., Marshall, S., Minniti, D., Nelson, C., Peterson, B., Popowski, P., Pratt, M., Quinn, P., Rodgers, A., Stubbs, C., Sutherland, W., Vandehei, T., & Welch, D. L. 2003, ApJ, 598, 597

Ashley, M. C. B., Allen, G., Bonner, C. S., Bradley, S. G., Cui, X., Everett, J. R., Feng, L., Gong, X., Hengst, S., Hu, J., Jiang, Z., Kulesa, C. A., Lawrence, J. S., Li, Y., Luong-Van, D. M., McCaughrean, M. J., Moore, A. M., Pennypacker, C., Qin, W., Riddle, R., Shang, Z., Storey, J. W. V., Sun, B., Suntzeff, N., Tothill, N. F. H., Travouillon, T., Walker, C. K., Wang, L., Yan, J., Yang, H., York, D. G., Yuan, X., Zhang, X., Zhang, Z., Zhou, X., & Zhu, Z. 2010, Highlights of Astronomy, 15, 627

Baglin, A., Auvergne, M., Boisnard, L., Lam-Trong, T., Barge, P., Catala, C., Deleuil, M., Michel, E., & Weiss, W. 2006, in 36th COSPAR Scientific Assembly, Vol. 36, 3749–+

Benkő, J. M., Kolenberg, K., Szabó, R., Kurtz, D. W., Bryson, S., Bregman, J., Still, M., Smolec, R., Nuspl, J., Nemec, J. M., Moskalik, P., Kopacki, G., Kolláth, Z., Guggenberger, E., di Criscienzo, M., Christensen-Dalsgaard, J., Kjeldsen, H., Borucki, W. J., Koch, D., Jenkins, J. M., & van Cleve, J. E. 2010, MNRAS, 409, 1585

Blažko, S. 1907, Astronomische Nachrichten, 175, 325

Boisnard, L. & Auvergne, M. 2006, in ESA Special Publication, Vol. 1306, ESA Special Publication, ed. M. Fridlund, A. Baglin, J. Lochard, & L. Conroy, 19–+

Bonner, C. S., Ashley, M. C. B., Cui, X., Feng, L., Gong, X., Lawrence, J. S., Luong-van, D. M., Shang, Z., Storey, J. W. V., Wang, L., Yang, H., Yang, J., Zhou, X., & Zhu, Z. 2010, PASP, 122, 1122

Borucki, W. J., Koch, D., Basri, G., & et al. 2010, Science, 327, 977

Breger, M. 2000, in Astronomical Society of the Pacific Conference Series, Vol. 210, Delta Scuti and Related Stars, ed. M. Breger & M. Montgomery, 3–+

Buchler, J. R. & Kolláth, Z. 2011, ApJ, 731, 24

Burton, M. G. 2010, A&A Rev., 18, 417

Crouzet, N., Guillot, T., Agabi, A., Rivet, J.-P., Bondoux, E., Challita, Z., Fanteï-Caujolle, Y., Fressin, F., Mékarnia, D., Schmider, F.-X., Valbousquet, F., Blazit, A., Bonhomme, S., Abe, L., Daban, J.-B., Gouvret, C., Fruth, T., Rauer, H., Erikson, A., Barbieri, M., Aigrain, S., & Pont, F. 2010, A&A, 511, A36+

Cui, X., Yuan, X., & Gong, X. 2008, in Society of Photo-Optical Instrumentation Engineers (SPIE) Conference Series, Vol. 7012, Society of Photo-Optical Instrumentation Engineers (SPIE) Conference Series

Cuypers, J., Aerts, C., De Cat, P., De Ridder, J., Goossens, K., Schoenaers, C., Uytterhoeven, K., Acke, B., Davignon, G., Debosscher, J., Decin, L., De Meester, W., Deroo, P., Drummond, R., Kolenberg, K., Lefever, K., Raskin, G., Reyniers, M., Saesen, S., Vandenbussche, B., van Malderen, R., Verhoelst, T., van Winckel, H., & Waelkens, C. 2009, A&A, 499, 967

Fukugita, M., Ichikawa, T., Gunn, J. E., Doi, M., Shimasaku, K., & Schneider, D. P. 1996, AJ, 111, 1748

Hengst, S., Allen, G. R., Ashley, M. C. B., Everett, J. R., Lawrence, J. S., Luong-Van, D. M., & Storey, J. W. V. 2008, in Presented at the Society of Photo-Optical Instrumentation Engineers (SPIE) Conference, Vol. 7012, Society of Photo-Optical Instrumentation Engineers (SPIE) Conference Series

Jurcsik, J., Sódor, Á., Szeidl, B., Hurta, Z., Váradi, M., Posztobányi, K., Vida, K., Hajdu, G., Kővári, Z., Nagy, I., Molnár, L., & Belucz, B. 2009, MNRAS, 400, 1006

Kaluzny, J., Stanek, K. Z., Krockenberger, M., Sasselov, D. D., Tonry, J. L., & Mateo, M. 1998, AJ, 115, 1016

Kaye, A. B., Handler, G., Krisciunas, K., Poretti, E., & Zerbi, F. M. 1999, PASP, 111, 840

Kenyon, S. L., Lawrence, J. S., Ashley, M. C. B., Storey, J. W. V., Tokovinin, A., & Fossat, E. 2006, PASP, 118, 924

Kenyon, S. L. & Storey, J. W. V. 2006, PASP, 118, 489

Kovács, G., Zucker, S., & Mazeh, T. 2002, A&A, 391, 369

Lasker, B. M., Lattanzi, M. G., McLean, B. J., Bucciarelli, B., Drimmel, R., Garcia, J., Greene, G., Guglielmetti, F., Hanley, C., Hawkins, G., Laidler, V. G., Loomis, C., Meakes, M., Mignani, R., Morbidelli, R., Morrison, J., Pannunzio, R., Rosenberg, A., Sarasso, M., Smart, R. L., Spagna, A., Sturch, C. R., Volpicelli, A., White, R. L., Wolfe, D., & Zacchei, A. 2008, AJ, 136, 735

Lawrence, J. S., Allen, G. R., Ashley, M. C. B., Bonner, C., Bradley, S., Cui, X., Everett, J. R., Feng, L., Gong, X., Hengst, S., Hu, J., Jiang, Z., Kulesa, C. A., Li, Y., Luong-Van, D., Moore, A. M., Pennypacker, C., Qin, W., Riddle, R., Shang, Z., Storey, J. W. V., Sun, B., Suntzeff, N., Tothill, N. F. H., Travouillon, T., Walker, C. K., Wang, L., Yan, J., Yang, J., Yang, H., York, D., Yuan, X., Zhang, X. G., Zhang, Z., Zhou, X., & Zhu, Z. 2008, in Presented at the Society of Photo-Optical Instrumentation Engineers (SPIE) Conference, Vol. 7012, Society of Photo-Optical Instrumentation Engineers (SPIE) Conference Series

Lawrence, J. S., Ashley, M. C. B., Burton, M. G., Cui, X., Everett, J. R., Indermuehle, B. T., Kenyon, S. L., Luong-Van, D., Moore, A. M., Storey, J. W. V., Tokovinin, A., Travouillon, T., Pennypacker, C., Wang, L., & York, D. 2006, in Presented at the Society of Photo-Optical Instrumentation Engineers (SPIE) Conference, Vol. 6267, Society of Photo-Optical Instrumentation Engineers (SPIE) Conference Series

Lawrence, J. S., Ashley, M. C. B., Hengst, S., Luong-Van, D. M., Storey, J. W. V., Yang, H., Zhou, X., & Zhu, Z. 2009, Rev Sci Instrum, 80, 064501

Lenz, P. & Breger, M. 2005, Communications in Asteroseismology, 146, 53
Lomb, N. R. 1976, Ap&SS, 39, 447
Luong-van, D. M., Ashley, M. C. B., Cui, X., Everett, J. R., Feng, L., Gong, X., Hengst, S., Lawrence, J. S., Storey, J. W. V., Wang, L., Yang, H., Yang, J., Zhou, X., & Zhu, Z. 2010, in Presented at the Society of Photo-Optical Instrumentation Engineers (SPIE) Conference, Vol. 7733, Society of Photo-Optical Instrumentation Engineers (SPIE) Conference Series
Monet, D. G., Levine, S. E., Canzian, B., Ables, H. D., Bird, A. R., Dahn, C. C., Guetter, H. H., Harris, H. C., Henden, A. A., Leggett, S. K., Levison, H. F., Luginbuhl, C. B., Martini, J., Monet, A. K. B., Munn, J. A., Pier, J. R., Rhodes, A. R., Riepe, B., Sell, S., Stone, R. C., Vrba, F. J., Walker, R. L., Westerhout, G., Brucato, R. J., Reid, I. N., Schoening, W., Hartley, M., Read, M. A., & Tritton, S. B. 2003, AJ, 125, 984
Mosser, B. & Aristidi, E. 2007, PASP, 119, 127
Ofek, E. O. 2008, PASP, 120, 1128
Paczyński, B., Szczygieł, D. M., Pilecki, B., & Pojmański, G. 2006, MNRAS, 368, 1311
Pojmanski, G. 2005, VizieR On-line Data Catalog: J/other/AcA/50.177. Originally published in: 2000AcA....50..177P, 50, 5001
Riaz, B., Gizis, J. E., & Harvin, J. 2006, AJ, 132, 866
Samus, N. N., Durlevich, O. V., & et al. 2009, VizieR Online Data Catalog, 1, 2025
Saunders, W., Lawrence, J. S., Storey, J. W. V., Ashley, M. C. B., Kato, S., Minnis, P., Winker, D. M., Liu, G., & Kulesa, C. 2010, in EAS Publications Series, Vol. 40, EAS Publications Series, ed. L. Spinoglio & N. Epchtein, 89–96
Saunders, W., Lawrence, J. S., Storey, J. W. V., Ashley, M. C. B., Kato, S., Minnis, P., Winker, D. M., Liu, G., & Kulesa, C. 2009, PASP, 121, 976
Scargle, J. D. 1982, ApJ, 263, 835
Smith, H. 1995, RR Lyrae Stars (Cambridge Univ. Press)
Stetson, P. B. 1987, PASP, 99, 191
—. 1996, PASP, 108, 851
Storey, J. W. 2009, Assoc Asia Pac Phys Soc Bull, 19, 4
Storey, J. W. V. 2005, Antarctic Science, 17, 555
—. 2007, Chinese Astron. Astrophys., 31, 98
Strassmeier, K. G., Briguglio, R., Granzer, T., Tosti, G., Divarano, I., Savanov, I., Bagaglia, M., Castellini, S., Mancini, A., Nucciarelli, G., Straniero, O., Distefano, E., Messina, S., & Cutispoto, G. 2008, A&A, 490, 287
Swain, M. R. & Gallée, H. 2006, PASP, 118, 1190
Taylor, M. 1990, AJ, 100, 1264
Wright, C. O., Egan, M. P., Kraemer, K. E., & Price, S. D. 2003, AJ, 125, 359
Yang, H., Allen, G., Ashley, M. C. B., Bonner, C. S., Bradley, S., Cui, X., Everett, J. R., Feng, L., Gong, X., Hengst, S., Hu, J., Jiang, Z., Kulesa, C. A., Lawrence, J. S., Li, Y., Luong-van, D., McCaughrean, M. J., Moore, A. M., Pennypacker, C., Qin, W., Riddle, R., Shang, Z., Storey, J. W. V., Sun, B., Suntzeff, N., Tothill, N. F. H., Travouillon, T., Walker, C. K., Wang, L., Yan, J., Yang, J., York, D., Yuan, X., Zhang, X., Zhang, Z., Zhou, X., & Zhu, Z. 2009, PASP, 121, 174
Yuan, X., Cui, X., Liu, G., Zhai, F., Gong, X., Zhang, R., Xia, L., Hu, J., Lawrence, J. S., Yan, J., Storey, J. W. V., Wang, L., Feng, L., Ashley, M. C. B., Zhou, X., Jiang, Z., & Zhu, Z. 2008, in Society of Photo-Optical Instrumentation Engineers (SPIE) Conference Series, Vol. 7012, Society of Photo-Optical Instrumentation Engineers (SPIE) Conference Series
Zhou, X., Fan, Z., Jiang, Z., Ashley, M. C. B., Cui, X., Feng, L., Gong, X., Hu, J., Kulesa, C. A., Lawrence, J. S., Liu, G., Luong-Van, D. M., Ma, J., Moore, A. M., Qin, W., Shang, Z., Storey, J. W. V., Sun, B., Travouillon, T., Walker, C. K., Wang, J., Wang, L., Wu, J., Wu, Z., Xia, L., Yan, J., Yang, J., Yang, H., Yuan, X., York, D., Zhang, Z., & Zhu, Z. 2010a, PASP, 122, 347
Zhou, X., Wu, Z., Jiang, Z., Cui, X., Feng, L., Gong, X., Hu, J., Li, Q., Liu, G., Ma, J., Wang, J., Wang, L., Wu, J., Xia, L., Yan, J., Yuan, X., Zhai, F., Zhang, R., & Zhu, Z. 2010b, Research in Astronomy and Astrophysics, 10, 279
Zou, H., Zhou, X., Jiang, Z., Ashley, M. C. B., Cui, X., Feng, L., Gong, X., Hu, J., Kulesa, C. A., Lawrence, J. S., Liu, G., Luong-Van, D. M., Ma, J., Moore, A. M., Pennypacker, C. R., Qin, W., Shang, Z., Storey, J. W. V., Sun, B., Travouillon, T., Walker, C. K., Wang, J., Wang, L., Wu, J., Wu, Z., Xia, L., Yan, J., Yang, J., Yang, H., Yao, Y., Yuan, X., York, D. G., Zhang, Z., & Zhu, Z. 2010, AJ, 140, 602

APPENDIX

TABLE A1
Fourier Analysis of Variable Star Candidates

CSTAR ID	Freq. [c/d]	Amp. [mmag]	S/N	Notes
000572	6.475955	60.74	11.04	
	16.964241	11.56	4.26	
001707	5.907794	259.90	19.84	f1
	11.815589	94.63	19.71	2f1
	17.723383	43.02	20.49	3f1
	23.631178	16.74	18.22	4f1
	2.953241	13.88	7.30	0.5f1
	29.539444	7.67	15.23	5f1
003125	0.278487	22.41	8.53	f1
	0.139674	16.74	8.38	0.5f1
	5.016641	5.56	4.27	
003697	0.037071	33.69	13.28	
004463	2.303088	7.66	4.74	f1
	5.013947	9.09	5.98	
	4.604452	6.45	5.49	2f1
	6.905816	6.21	6.45	3f1
	9.206318	4.97	6.43	4f1
	11.510546	3.98	7.64	5f1
	13.812341	2.76	6.52	6f1
	13.032144	2.50	6.10	
	16.113611	2.18	5.81	7f1
	26.071184	1.27	4.27	
	34.092800	1.02	4.33	
005954	0.013361	37.42	16.30	
	0.051720	10.34	7.87	
008426	0.113784	10.93	7.71	
009171	1.690393	270.20	10.48	f1
	3.380355	139.87	10.87	2f1
	5.070748	90.51	10.35	3f1
	6.761141	67.58	10.71	4f1
	8.451533	42.15	9.40	5f1
	10.141927	20.77	5.92	6f1
009952	0.042238	30.29	11.46	
011616	0.031463	17.31	10.59	
011709	0.339196	23.99	13.45	f1
	0.675806	7.24	7.16	2f1
011796	1.057236	67.40	11.70	f1
	2.114041	40.08	11.25	2f1
	3.171277	30.60	11.68	3f1
	0.528834	30.16	10.52	0.5f1
	1.585208	22.13	11.80	1.5f1
	4.228082	18.44	11.99	4f1
	2.642013	18.03	13.69	2.5f1
	3.699680	12.52	13.01	3.5f1
	5.285318	9.32	14.17	5f1
	4.756054	6.72	12.99	4.5f1
013140	0.048703	19.44	11.78	
	0.021550	7.78	7.46	
013432	0.013367	26.49	9.41	
	0.040102	18.95	7.52	
	0.073305	11.12	4.96	
	5.012740	8.36	6.03	
014111	5.744743	172.54	17.85	f1
	11.489056	27.26	10.16	2f1
	2.868061	15.18	4.39	0.5f1
014495	0.053444	25.15	14.02	
	0.037066	6.09	6.47	
016836	5.675009	122.96	23.33	f1
	0.102148	20.23	6.06	
	11.350019	17.23	13.80	2f1
	0.070684	16.05	5.12	
	17.026321	5.29	5.39	3f1
018708	1.228764	15.06	7.68	f1
	2.457959	9.67	6.90	2f1
	3.687154	7.94	6.86	3f1
	0.614382	7.48	5.86	0.5f1
	28.365950	4.86	10.15	
	4.916780	3.88	5.57	4f1
	24.912863	2.18	4.95	
	1.057168	4.68	5.16	
	27.730873	2.04	4.85	
	1.173146	3.23	3.42	
	11.060168	1.82	4.01	9f1
	9.833129	2.36	5.12	8f1
	25.758816	1.47	3.92	
	26.705179	1.34	3.75	
	4.298518	2.36	3.38	3.5f1
	8.602209	1.64	3.73	7f1
	24.896910	1.47	3.54	
	23.724195	1.65	4.52	
020436	0.018113	115.20	14.09	
	0.027600	23.34	9.13	
020526	0.796911	133.14	13.22	f1
	1.593822	50.02	10.83	2f1
	1.195151	34.28	9.21	1.5f1
	0.398671	30.44	9.87	0.5f1
022489	3.066545	107.03	25.84	f1
	6.132659	7.88	37.04	2f1
	1.533057	7.63	9.71	0.5f1
	4.599602	4.20	10.45	1.5f1
	3.059649	3.89	6.19	
	9.199203	2.17	10.60	3f1
023885	0.575379	3.02	5.34	
025440	0.101715	3.72	7.21	
	0.210326	3.16	7.30	
025846	0.101716	27.26	8.53	
026640	0.020257	31.03	12.39	
	0.009482	37.92	13.69	
	0.036635	10.34	8.42	
	0.053013	6.14	6.53	
026730	0.967161	11.96	8.56	f1
	2.904499	8.66	7.85	3f1
	4.840114	7.44	8.12	5f1
	1.936046	8.39	6.32	2f1
	3.872522	8.02	7.83	4f1
	6.776160	5.37	7.93	7f1
	2.419195	6.48	6.11	2.5f1
	5.808568	6.17	7.74	6f1
	0.483149	5.71	5.35	0.5f1
	7.744183	5.59	8.85	8f1
	4.356534	4.98	7.14	4.5f1
027082	0.150418	2.85	6.26	
027575	0.162054	5.04	6.59	
	0.074562	4.74	6.66	
	0.179294	2.99	5.65	
028221	0.206017	71.45	13.86	
	0.026722	9.72	4.83	
	0.102146	10.48	4.45	
029379	0.322387	23.21	7.89	
030353	0.955090	46.94	15.46	
	1.024911	5.72	4.49	
	28.078613	1.68	4.01	
032007	1.608054	44.58	16.98	f1
	3.215677	15.04	11.48	2f1
	1.645551	12.70	7.01	f3
	4.823300	6.18	9.95	3f1
	1.571419	5.78	4.32	f2
	3.253174	6.09	5.92	2f3
	4.861228	4.86	7.27	3f3
	6.469282	4.11	9.72	4f1
032544	0.036635	17.74	17.24	
	0.044393	6.70	8.61	
	0.057754	4.91	8.21	
	0.021119	6.40	15.52	
034389	0.576245	24.15	7.39	
034669	0.068097	19.74	13.55	
	0.061201	6.87	9.08	
	0.010344	3.81	7.02	
034724	0.024136	65.58	14.39	f1
	0.048272	15.11	8.82	2f1

TABLE A1 — *Continued*

CSTAR ID	Freq. [c/d]	Amp. [mmag]	S/N	Notes
	0.030601	9.54	6.71	
	0.056892	6.71	5.54	
034997	1.546844	227.25	19.62	f1
	3.093256	122.24	19.93	2f1
	4.640100	79.59	20.65	3f1
	6.186513	52.77	22.37	4f1
	7.733357	26.78	20.52	5f1
	9.279770	16.35	19.04	6f1
	10.826613	10.94	17.50	7f1
	12.373026	5.82	14.94	8f1
	1.539948	7.04	6.56	
035468	2.430840	15.96	6.73	f1
	7.292090	9.30	6.18	3f1
	4.861250	8.85	6.21	2f1
	9.721638	8.65	6.93	4f1
036162	2.289026	63.01	16.56	f1
	1.144729	34.01	12.84	0.5f1
	4.577621	29.43	14.61	2f1
	3.433323	25.90	17.49	1.5f1
	6.866647	18.35	15.33	3f1
	5.722350	17.01	20.09	2.5f1
	8.010513	9.12	15.74	3.5f1
	9.155673	7.67	17.89	4f1
036508	0.026729	85.37	10.56	
	3.958093	18.96	4.52	
036939	0.135333	8.50	8.41	
037016	6.331342	29.84	18.14	
037271	0.006896	17.65	7.69	
	0.076286	15.95	5.71	
	0.065080	11.36	4.93	
038255	7.493285	239.91	27.40	f1
	14.986570	70.71	27.40	2f1
	22.480286	21.95	23.99	3f1
	3.746643	17.78	14.17	0.5f1
	0.935260	7.69	4.73	
	0.988703	7.97	5.10	
	37.466766	4.13	10.37	5f1
	26.226521	3.66	9.09	3.5f1
	6.017149	3.44	5.70	
	7.502790	3.24	5.50	
	44.960915	3.00	7.94	6f1
	33.718830	2.80	7.88	4.5f1
	14.995214	2.72	5.64	
038580	0.143522	7.60	7.78	
	0.174122	6.88	7.28	
038663	7.487258	227.63	27.71	f1
	14.974086	64.44	26.97	2f1
	3.743629	28.80	24.60	0.5f1
	22.461344	25.91	26.46	3f1
	11.230456	14.91	24.69	1.5f1
	18.718145	9.14	23.23	2.5f1
	29.948694	6.86	21.60	4f1
	7.479931	5.35	12.48	
	26.204634	3.04	14.97	3.5f1
	3.753542	2.74	8.33	
	14.965915	1.71	8.66	
	7.493742	3.52	6.06	
	7.502361	2.30	9.23	
	37.435745	1.55	8.87	5f1
	7.472192	1.43	4.68	
	9.022915	0.96	4.68	
	13.035054	0.93	4.72	
	14.981862	1.19	4.99	
	33.692978	0.87	5.42	4.5f1
	7.463141	1.08	3.79	
039541	0.072838	13.94	14.34	
	0.044392	5.18	6.17	
	0.017240	4.42	7.19	
	0.090509	3.55	6.86	
040351	3.501848	25.48	17.69	
	3.477713	19.49	16.44	
042081	0.159469	6.45	9.15	
042266	5.219686	183.05	17.38	f1
	10.439812	49.96	5.83	2f1
	15.658175	19.28	8.27	3f1

TABLE A1 — *Continued*

CSTAR ID	Freq. [c/d]	Amp. [mmag]	S/N	Notes
	25.066116	9.26	4.50	5f1-1
043618	0.153436	92.61	13.78	f1
	0.308595	37.63	8.33	2f1
	0.461600	33.14	7.75	3f1
	0.615467	22.20	7.15	4f1
	0.077149	21.86	6.65	0.5f1
	0.768902	13.83	6.63	5f1
	0.229292	13.74	6.44	1.5f1
	0.380141	12.41	4.79	2.5f1
043885	0.106025	50.37	12.65	
044751	0.153434	14.38	10.57	
047176	0.380418	40.79	11.63	f1
	0.762992	10.60	6.09	2f1
048452	0.100422	19.16	10.39	
	0.173261	7.87	5.50	
048615	0.343072	10.86	7.56	
050375	0.693901	27.68	11.98	
	0.035342	8.66	5.69	
	0.103008	5.76	4.33	
050773	0.306100	23.02	8.15	f1
	0.612632	10.47	4.75	2f1
052891	0.018533	64.30	20.88	
	0.071545	5.00	5.81	
	0.029308	5.97	5.77	
	0.057753	5.19	4.55	
	0.208171	3.27	4.36	
053446	0.933536	27.67	11.48	f1
	1.871813	15.00	8.98	2f1
	0.103008	8.83	5.23	
053570	0.051288	5.50	9.98	
	0.075855	2.84	6.28	
053783	0.060770	3.45	8.76	f1
	0.123265	2.26	6.27	2f1
055495	2.506240	134.34	20.81	f1
	1.253336	61.92	17.65	0.5f1
	5.012481	55.40	19.32	2f1
	3.759576	34.08	21.97	1.5f1
	7.518721	23.69	18.48	3f1
	6.265816	17.99	21.71	2.5f1
	8.772057	6.93	14.34	3.5f1
	10.025393	5.24	13.85	4f1
	0.100853	2.99	4.55	
	11.277453	2.04	6.68	4.5f1
	16.043404	2.00	6.15	6.4f1
	15.034443	1.82	5.98	6f1
	7.019646	1.40	4.26	2.8f1
	40.113522	1.32	4.66	16f1
055854	0.017240	8.42	10.33	
	0.059478	10.44	8.22	
	0.026722	7.40	7.66	
	0.070683	4.89	6.36	
	0.040945	4.52	6.05	
057247	0.024136	103.94	15.85	
057344	0.048702	29.96	12.44	
	0.036204	14.65	12.65	
	0.010344	12.20	11.31	
	0.018964	4.96	6.98	
	0.089216	4.77	5.86	
057775	4.559935	186.04	27.32	f1
	9.119870	42.91	26.41	2f1
	13.679375	14.87	25.22	3f1
	6.839903	4.85	13.70	1.5f1
	2.278675	2.85	4.68	0.5f1
	4.553039	3.18	6.48	f2
	18.239328	1.98	9.93	4f1
	15.957636	1.21	6.81	3.5f1
	9.112992	1.43	5.14	2f2
	20.518433	1.03	6.06	4.5f1
059811	0.551742	27.24	5.13	f1
	1.103485	26.13	5.69	2f1
	1.655227	22.77	5.53	3f1
	0.275871	27.04	5.52	0.5f1
	0.828044	24.20	6.17	1.5f1
	1.379356	22.14	6.38	2.5f1
	1.931529	20.21	6.33	3.5f1

TABLE A1 — *Continued*

CSTAR ID	Freq. [c/d]	Amp. [mmag]	S/N	Notes
	2.207400	19.30	6.47	4f1
	2.758711	16.57	5.97	5f1
	2.482840	16.22	5.91	4.5f1
	3.034582	14.31	5.75	5.5f1
	3.310885	13.31	5.69	6f1
	3.586325	10.94	5.31	6.5f1
	3.862627	9.52	4.89	7f1
061353	44.287922	2.11	15.79	
	44.168968	1.62	15.75	
	42.120911	1.18	15.07	
	37.660107	0.36	5.56	
	39.444427	0.35	5.65	
	42.308395	0.25	4.23	
	45.354671	0.23	3.74	
061658	13.129424	4.07	19.30	
	23.308718	2.03	11.76	
	22.974697	1.24	8.36	
	16.556738	1.07	8.14	
	20.022375	0.95	7.00	
	26.205441	0.92	7.64	
	23.396641	0.80	6.37	
	18.800934	0.73	6.03	
	11.388237	0.69	5.61	
	10.866733	0.69	5.81	
	12.723462	0.52	4.86	
	23.211313	0.52	4.49	
061740	0.039651	8.28	11.18	
	0.090940	3.72	8.01	
	0.018533	7.11	7.18	
	0.055167	5.25	5.06	
061783	5.291335	81.82	18.91	
	8.022555	10.23	7.05	
	7.014887	6.97	4.20	
062683	0.044393	5.83	9.62	
	0.063357	7.04	8.23	
	0.028015	6.08	6.70	
	0.083182	4.41	7.10	
062854	0.029739	7.82	9.51	
063059	0.065945	6.78	8.60	
	0.032757	6.23	7.10	
	0.024568	5.12	5.12	
	0.075427	3.93	5.37	
	0.124994	2.48	5.03	
063241	7.595059	38.45	11.47	
	5.013037	12.85	4.73	
064380	0.432298	20.95	5.31	
	0.102579	15.94	4.47	
064944	0.080596	10.34	11.50	
	0.104301	7.13	8.34	
	0.054736	4.91	6.56	
	0.032756	3.38	4.23	
065072	1.611488	8.86	11.01	
	2.350212	7.61	11.21	
	2.673889	4.78	8.84	
	1.171443	4.16	7.17	
066196	0.021981	6.74	10.55	
	0.074131	7.30	8.36	
	0.061201	3.72	7.09	
	0.112490	3.69	6.39	
	0.096974	2.70	5.27	
066682	0.786142	9.78	5.42	
	0.103009	8.70	4.99	
066775	0.036635	34.98	14.47	
	0.010344	15.26	9.11	
	0.019395	15.08	13.33	
	0.056461	7.51	6.71	
	0.027584	14.51	5.06	
	0.086200	3.72	4.32	
	0.203862	2.77	4.60	
068276	0.357294	9.73	12.18	f1
	0.713296	3.88	7.16	2f1
068308	1.252474	14.79	8.00	
068493	0.074132	81.11	4.18	
068908	0.377984	4.51	8.38	
	0.368502	1.74	4.37	

TABLE A1 — *Continued*

CSTAR ID	Freq. [c/d]	Amp. [mmag]	S/N	Notes
	0.021981	1.45	4.26	
	0.352124	1.58	3.87	
069430	0.074997	76.28	12.56	
070680	1.006812	51.96	14.67	
	0.500389	23.21	9.49	
	2.014054	21.48	12.01	
	0.509009	13.26	9.84	
	3.018711	11.81	11.17	
	1.512803	8.11	7.83	
	2.517029	4.86	6.14	
	4.007421	4.91	6.04	
	1.502890	5.09	4.61	
	5.012939	3.52	5.48	
	0.057323	3.33	4.35	
070941	1.648985	9.23	8.97	
	1.600282	5.04	7.32	
	1.829140	2.84	4.60	
071571	0.034480	38.60	13.56	
	0.022843	30.81	10.19	
	0.084906	4.31	5.38	
072730	1.745096	183.43	18.05	f1
	3.490192	95.66	18.02	2f1
	5.235289	61.37	18.30	3f1
	6.980816	37.60	17.47	4f1
	8.725912	19.39	13.96	5f1
	1.732597	12.05	7.19	f2
	1.757595	12.05	9.28	f3
	10.470577	10.51	10.45	6f1
	3.502260	8.41	7.46	2f3
	5.247356	7.54	7.53	3f3
	6.993315	7.05	6.57	4f3
	12.215673	5.91	7.29	7f1
	6.968748	6.42	6.79	4f2
	5.222359	5.44	6.35	3f2
	8.022099	5.15	5.52	
	10.483938	3.87	5.14	6f3
	3.477694	4.03	5.09	2f2
	20.942879	3.62	4.73	12f1
	19.194765	3.57	4.90	11f1
	24.432209	3.56	4.75	14f1
	22.685820	3.42	4.93	13f1
	9.019851	3.61	4.78	
073028	0.103439	15.11	5.60	
073846	0.080165	5.91	10.40	
076723	0.019395	38.94	12.92	
	0.041807	36.84	7.73	
	0.059909	21.68	7.91	
	0.075856	18.13	7.96	
	0.092664	12.76	9.34	
	0.112059	7.73	9.01	
	0.122834	3.71	5.99	
	0.175847	2.32	5.27	
077171	0.176277	2.61	6.32	
077190	0.020257	5.03	8.09	
	0.048272	6.55	8.02	
	0.080165	4.90	7.21	
077508	7.501159	54.76	15.81	
077594	0.596069	3.91	10.88	
078549	0.185328	60.49	15.03	f1
	0.093957	9.05	6.32	0.5f1
078773	5.375379	30.51	26.14	f1
	2.687258	5.54	11.71	0.5f1
	0.013361	2.17	5.69	
	2.677777	1.98	6.74	
	2.697171	1.67	4.91	
	2.012750	1.72	5.39	
	0.958966	1.37	3.96	
	5.368483	1.16	4.13	
	6.017132	0.89	4.70	
	7.022645	0.66	3.89	
	8.062206	0.64	4.03	
	0.971033	1.22	3.61	
	18.047947	0.64	4.48	
	46.353683	0.51	4.09	
079397	0.206448	5.05	10.94	

TABLE A1 — *Continued*

CSTAR ID	Freq. [c/d]	Amp. [mmag]	S/N	Notes
	37.988960	1.24	11.76	
	32.580379	1.07	10.37	
	35.173904	1.01	10.74	
	32.170715	0.61	7.12	
	8.019998	0.51	6.08	
	35.604038	0.46	5.46	
	39.746784	0.44	5.38	
080934	0.015516	44.90	14.39	
	0.034480	19.99	13.38	
	0.024567	17.00	13.71	
	0.052151	3.41	4.95	
081428	0.093957	3.26	6.14	
	0.049996	2.68	5.04	
081563	0.042669	7.92	8.21	
081723	1.188292	20.55	9.77	
	1.299493	6.84	4.18	
	1.340869	5.42	3.58	
081749	0.014223	5.12	12.45	
082180	6.544276	4.83	18.95	f1
	0.027584	3.60	6.06	
	0.158176	2.42	4.79	
	0.074563	1.98	4.45	
	3.011984	1.36	5.25	
	4.012330	1.20	5.79	
	13.087427	1.08	7.51	2f1
082489	5.802769	173.02	15.26	f1
	2.900522	34.11	5.80	0.5f1
	11.605107	33.53	7.75	2f1
	17.407015	15.47	4.96	3f1
083110	0.024998	5.28	6.86	
	0.117231	3.02	5.79	
083768	5.207372	185.73	14.02	f1
	5.013339	26.76	9.42	
	10.414312	30.34	13.63	2f1
	7.022822	15.31	5.51	
	2.606279	10.40	5.15	0.5f1
	20.829922	8.56	8.71	4f1
	2.010348	7.57	4.37	
	26.036289	6.58	8.86	5f1
	7.811923	5.83	4.86	
	27.234083	3.17	5.54	
084344	0.681833	19.44	5.40	f1
	0.103870	15.75	5.39	
	0.343072	13.38	4.30	0.5f1
	0.025860	13.32	4.14	
085531	0.156886	30.31	8.04	
085719	0.060339	19.57	11.63	
	0.026291	11.90	9.69	
	0.086199	6.65	7.02	
	0.113783	4.37	5.20	
086480	0.098267	3.22	5.22	
	0.077148	2.65	4.77	
087084	1.076207	57.14	5.04	f1
	2.153707	46.23	4.85	2f1
	3.229483	38.13	4.92	3f1
	4.306552	35.92	6.69	4f1
	1.013281	27.29	4.42	
	0.534440	23.17	3.27	0.5f1
	5.383621	24.95	5.88	5f1
	6.458535	18.87	6.12	6f1
087501	5.168169	70.45	20.64	f1
	10.335475	8.13	6.08	2f1
	5.012145	5.68	4.97	
087548	5.057288	55.97	26.35	f1
	10.114145	6.42	14.67	2f1
	7.585932	3.24	9.01	
	15.171002	3.03	8.37	3f1
	13.037149	1.71	5.40	
088142	6.826951	147.51	25.30	f1
	13.654333	36.48	19.73	2f1
	0.064649	29.18	4.53	
	0.960256	29.40	5.02	
	20.481714	13.42	10.30	3f1
	0.207308	22.77	4.40	
	3.413044	14.68	5.05	0.5f1

TABLE A1 — *Continued*

CSTAR ID	Freq. [c/d]	Amp. [mmag]	S/N	Notes
	1.018871	20.22	4.24	
	0.440045	18.50	3.90	
	10.240857	6.84	5.27	1.5f1
	12.034657	5.75	4.83	
089391	7.305550	9.25	11.43	f1
	0.032756	4.93	4.89	
	0.170247	3.33	3.44	
	10.026622	2.91	4.19	
	14.614248	2.75	3.64	2f1
093873	0.029308	27.23	8.64	
	0.061202	23.25	9.51	
	0.018102	18.44	9.59	
	0.052151	14.87	9.76	
	0.076717	5.74	6.10	
	0.092664	5.47	5.74	
	0.121110	2.51	4.90	
094793	3.246138	10.17	4.60	
096404	1.718997	281.91	11.73	f1
	3.437994	152.42	14.47	2f1
	5.157423	92.84	13.79	3f1
	6.875988	63.18	12.98	4f1
	8.595848	37.14	10.38	5f1
	10.314413	24.19	7.21	6f1
	12.033411	17.12	6.25	7f1
097790	1.917082	4.44	13.08	
	1.874413	2.80	7.20	
	1.858897	1.36	4.96	
	2.017935	1.02	3.85	
098092	0.011206	58.09	16.75	
	0.026291	34.54	13.86	
	0.018533	15.87	9.68	
098719	4.802876	108.42	20.78	f1
	9.605320	22.83	18.49	2f1
	14.407334	7.77	12.48	3f1
099529	0.206448	3.35	6.18	
	0.043531	2.63	4.62	
	0.117231	2.06	4.97	
106019	0.031036	83.13	9.22	
	0.016811	29.97	7.61	
106769	0.040946	48.72	11.55	
107478	0.911567	42.45	7.09	f1
	1.823996	33.86	6.91	2f1
	2.735563	29.58	7.46	3f1
	3.647561	23.96	7.15	4f1
	0.453844	18.51	6.45	0.5f1
	1.368428	21.26	7.20	1.5f1
	2.280426	20.84	7.80	2.5f1
	3.192424	18.00	8.40	3.5f1
	4.559990	18.62	9.55	5f1
	4.103991	15.04	9.17	4.5f1
	5.471557	14.64	10.45	6f1
	5.015989	11.41	9.55	5.5f1
	6.383986	9.50	9.42	7f1
	0.462464	12.19	5.15	
	5.928418	8.44	10.24	6.5f1
	0.471946	7.60	5.10	
	0.444362	7.53	4.61	
	6.839554	5.84	9.18	7.5f1
	7.295984	4.87	9.14	8f1
110801	0.028015	34.27	14.13	
	0.011637	26.02	16.38	
	0.039652	8.21	7.22	
111298	0.083182	6.18	7.77	
	0.021981	5.45	7.12	
	0.104301	5.37	7.22	
113453	0.028446	10.70	8.95	
	0.074994	4.44	5.74	
114506	0.519781	8.08	6.39	
	0.534435	4.15	4.47	
116410	0.271096	8.72	6.95	
116471	3.798428	27.83	5.84	
117654	0.046117	27.08	12.46	
	0.058616	8.41	5.86	
	0.029308	8.93	7.01	

TABLE A1 — *Continued*

CSTAR ID	Freq. [c/d]	Amp. [mmag]	S/N	Notes
	0.011206	4.04	4.44	
118705	0.118095	13.83	8.44	
119488	0.012499	14.66	10.79	
	0.023705	11.98	8.62	
	0.031894	12.09	5.63	
	0.054737	8.77	6.89	
	0.062926	5.01	4.92	
120188	0.093527	10.44	9.82	
	0.081459	5.43	7.74	
	0.179726	3.37	4.91	
	4.011735	2.30	7.53	
121369	0.047410	10.20	9.89	
	0.012930	5.28	6.47	
	0.065512	3.74	5.43	
	0.080166	3.14	3.85	
121389	0.024577	37.09	8.41	
	0.044842	30.04	4.98	
	1.021869	17.90	4.20	
123934	8.195368	15.63	11.09	f1
	0.033619	7.85	4.96	
	6.017436	5.62	4.43	
	4.012774	4.97	3.97	
	16.390305	4.40	4.00	2f1
124666	2.183140	260.22	14.74	f1
	4.366280	106.12	15.01	2f1
	6.548989	58.61	14.30	3f1
	8.731267	28.31	10.96	4f1
	10.913976	17.01	9.17	5f1
	2.171933	16.61	4.51	f2
	2.191329	14.84	4.22	f3
	4.355936	13.15	5.33	2f2
	6.538213	11.71	6.46	3f2
	13.096254	9.98	7.99	6f1
	4.375762	8.86	4.12	2f3
	15.280687	7.11	7.00	7f1
	8.720106	6.64	4.94	4f2
	10.926521	6.57	5.09	5f3
	10.902021	5.66	4.91	5f2
	17.465235	5.05	5.22	8f1
	19.648375	4.90	5.38	9f1
	6.558585	5.41	3.80	3f3
	15.292439	4.73	4.94	7f3
128178	0.063889	61.37	11.47	
133742	2.357630	201.87	12.96	f1
	4.714828	61.60	10.89	2f1
	7.072026	26.21	8.52	3f1
	1.178384	24.54	5.30	0.5f1
	3.536875	16.25	4.72	1.5f1
	9.430688	5.97	4.44	4f1
	13.029390	6.70	5.15	5.5f1